

POLITECNICO DI TORINO

Collegio di Ingegneria Meccanica e Aerospaziale

**Corso di Laurea
in Ingegneria Meccanica**

Master Thesis

Design and control of a Prototype to Study Proprioception



INSA | INSTITUT NATIONAL
DES SCIENCES
APPLIQUÉES
LYON



Relatore

Carlo Ferraresi

Correlatori:

Minh Tu Pham

Richard Moreau

Candidato

Barbetta Giuseppina

Anno Accademico 2019/2020

*“Adieu, dit le renard. Voici mon secret.
Il est très simple : on ne voit bien qu’avec le cœur.
L’essentiel est invisible pour les yeux.”*

Le petit Prince - Antoine de Saint-Exupéry

Index

<i>Introduction</i>	5
<i>Proprioception</i>	6
<i>Mechanism</i>	10
<i>Biomechanics of upper limbs</i>	13
<i>Control behavior of CNS</i>	16
<i>Prototype</i>	18
<i>Default values</i>	19
<i>Description of the project</i>	20
<i>Device specifications</i>	21
<i>First prototype</i>	23
<i>State of the art and design ideas</i>	24
<i>Resolutions - Design and connections of the arm support</i>	26
<i>Motorization of the system</i>	27
<i>Final solution</i>	29
<i>Cable control</i>	33
<i>Prototype production</i>	34
<i>Rotation sensors</i>	35
<i>The motors</i>	38
<i>Trajectory calculation</i>	40
<i>The controls</i>	44
<i>Zettlex IncOder</i>	46
<i>Design of pieces to block and change rotations</i>	54
<i>Control</i>	61
<i>Execution of tests</i>	73
<i>Geometrical tests</i>	80

<i>Arduino</i>	85
<i>Conclusion</i>	91
<i>Bibliography</i>	93
<i>Appendix</i>	97
<i>Appreciation</i>	101

Introduction

As part of my formation as Mechanical Engineering Master's Degree student at the “Politecnico di Torino” and Erasmus student at INSA LYON, I chose to carry out my final Thesis project at the Ampere Laboratory of INSA LYON.

The Laboratory combines automatic and mechanical design activities, which aroused my interest for the mechatronic aspect, still unknown to me and specially very innovative.

Following a collaboration between CRNL (Lyon Neuroscience Research Center), INSERM (Institut National de la Santé Et de la Recherche Médicale) and Ampère laboratory, INSA Lyon, a first prototype was designed and manufactured and then continued by two INSA students as part of a PFE in 2017. This prototype aims to set up experimental protocols to test proprioception in humans. Proprioception is the perception, conscious or not, of the position of the different parts of the body. This prototype consists of two symmetrical parts to measure and move the position of the limbs of a subject during movements in the sagittal and horizontal planes.

The expected work is to improve the current prototype. Indeed, following several tests with researchers at CRNL, some areas for improvement have been mentioned.

These are mainly:

1. Review the design of certain parts that do not allow for simple adjustments;
2. Complete the motor control part to follow the movement of the limb when the subject is active;
3. Implementation of new sensors to obtain more precise data about the position of the mechanical arms;
4. Improve the overall ergonomics of the prototype;
5. Improve overall safety for both the subject and the operator.

This work is therefore very multidisciplinary and requires skills in terms of design and control of a mechatronic system. I had to work in a team with both the researchers of the Ampère laboratory but also with those of the CRNL.

Proprioception

The proprioception, or deep sensitivity, refers to the perception unconscious of the position of different parts of the body, of movement and spatial orientation providing CNS information about. It works with many muscle receptors, ligaments and with the pathways and nerve centers involved.

In vertebrates, limb speed and movement are encrypted by one group of sensory neurons (Type Ia sensory fiber) and another type encode static muscle length (Group II neurons). “These two types of sensory neurons compose muscle spindles” [29].

Muscle spindles are small sensory receptors within the muscle. As the muscle spindles lay in the muscle parallel to the muscle fibres, its stretch is proportional to the stretch of the muscle. The main components of a muscle spindle are the intrafusal muscle fibres, afferent sensory fibre endings and efferent motor fibre endings. The sensory fibres endings spiral around the central region of the intrafusal muscle fibres and are responsive to stretch of these muscle fibres. γ -motoneurons innervate the intrafusal muscle fibres and changes the sensitivity of the sensory fibre endings to stretch.

A muscle spindle contains three types of intrafusal muscle fibres: dynamic nuclear bag fibres, static nuclear bag fibres, and nuclear chain fibres. Two types of afferent sensory fibres leave the muscle spindle: primary (Ia) and secondary (II) endings. Primary endings are most sensitive to stretch velocity and secondary endings to stretch. Primary endings make contact with all three types of intrafusal muscle fibres, the secondary ending make contact with static nuclear bag and nuclear chain fibres.

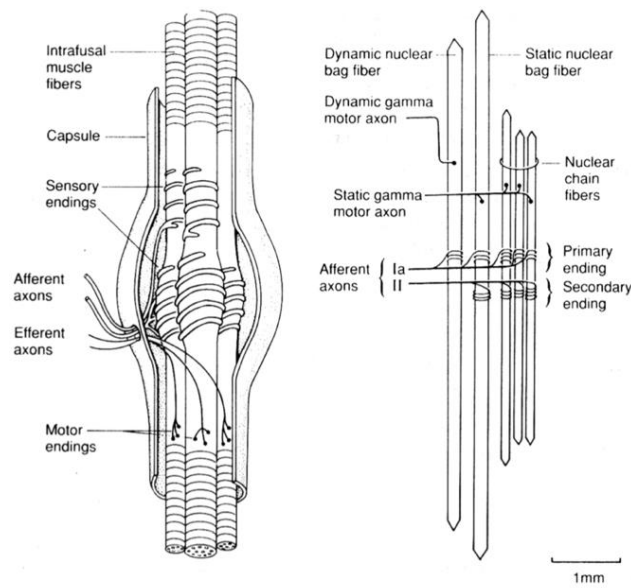


Fig.3 – Muscle fibres

“To determine the load on a limb, vertebrates use sensory neurons in the Golgi tendon organs: type Ib afferents. These proprioceptors are activated at given muscle forces, which indicate the resistance that muscle is experiencing” [9].

Golgi tendon organs (GTOs) are sensory receptors located at the junction between muscle fibres and tendon. Tendon organs are thin encapsulated structures and have one single afferent axon (Ib). The afferent ending diverges into many fine endings, which intertwines among the collagen fibres. Stretching of a GTO straightens the collagen fibres, compressing the nerve endings and causes them to fire. The stretch of a GTO depends on the load, which is proportional to the muscle force, as a GTO is in series with a muscle.

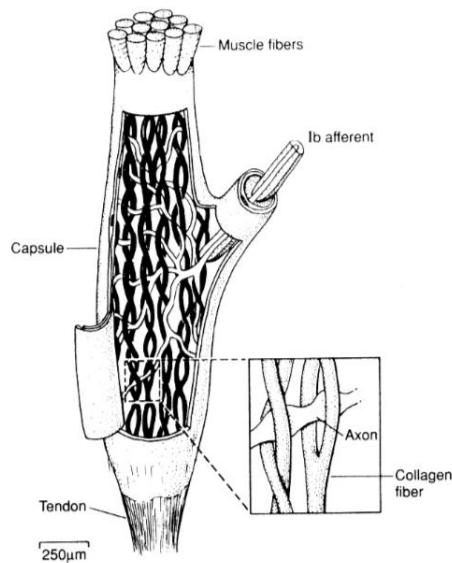


Fig.4 – Golgi tendon organs (GTOs)

A third role for proprioceptors is to determine when a joint is in a particular position. In vertebrates, this is performed by Ruffini endings and Pacinian corpuscles. These proprioceptors are activated when the joint is at a margin, usually at the extremes of joint position.

In human motion control one tries to identify the dynamics of the skeleton, muscles, sensors, and controller. It is the challenge to find the structure and the parameters of the controller and how it handles with different conditions and/or disturbances.

Position, forces and EMG of the muscles are the variables that can be observed noninvasively in humans. Furthermore, position and force disturbances can be applied to perturb the posture and to provoke a response. With system identification a model of the system (joint dynamics) is obtained by analysis between input (position or force) and output (force or position, sometimes EMG). Two types of perturbations (input) can be distinguished, i.e. force and position perturbations. For technical systems there is no principal difference. However, humans are highly adaptive and need a proper task instruction. Force disturbances require a position task and vice versa.

Position tasks (with force variations) are natural for the subject. They mimic daily life situations and are superior to investigate the functionality of proprioceptive reflexes. The subject has to actively preserve stability and reflexes contribute to the performance. Note

that in human motion control the function of the perturbation is twofold. Firstly it provides information necessary to excite the system, allowing identification, and secondly the perturbation is part of the conditions to direction reflexive behaviour. As the CNS is an adaptive controller, weighting performance against effort, different perturbations will give different weights.

The neuromusculoskeletal system is highly nonlinear by nature, as the skeleton is a multi-link system and the muscles, proprioceptors, and neurons are all non-linear. Most control engineering and system identification tools are only valid for linear systems. It is desirable to investigate the human neuromusculoskeletal system in a state that allows linearization, so that linear tools can be used. Linearization is allowed when small deviations around an equilibrium posture are concerned, for example during postural control.

Proprioceptors can plan reflex circuits with motor neurons to produce speedy feedback regarding body and limb position. These mechanosensory circuits are significant for flexibly maintaining posture and balance, particularly throughout locomotion. As an example, examine the stretch reflex, in which stretch across a muscle is detected by a sensory receptor (e.g., muscle spindle, chordotonal neurons), which activates a motor neuron to induce muscle contraction and oppose the stretch. During locomotion, sensory neurons can reverse their action when stretched, to aid rather than oppose movement.

In humans, a differentiation is formed between conscious proprioception and non-conscious proprioception:

- Conscious proprioception is communicated by the dorsal column-medial lemniscus pathway to the cerebrum.
- Non-conscious proprioception is communicated primarily via the dorsal spinocerebellar tract and ventral spinocerebellar tract, to the neural structure.

A non-conscious reaction is visible in the human proprioceptive reflex, or righting reflex—if the body slants in any direction, the person will tilt their head back to level the eyes beside the horizon. This is observable even in infants as soon as they gain control of their neck muscles. This control comes from the cerebellum, the part of the brain involving balance.

Mechanism

Proprioception is mediated by mechanically sensitive proprioceptor neurons allocated throughout the body. Most vertebrates own three basic types of proprioceptors: muscle spindles, which are insert in skeletal muscle fibers, Golgi tendon organs, which are situated at the interface of muscles and tendons, and joint receptors, which are low-threshold mechanoreceptors fixed in joint capsules.

The first appearance of proprioception is the activation of a proprioceptor in the periphery. The proprioceptive sense is assumed to be composed of messages from sensory neurons located in the inner ear (motion and orientation) and in the stretch receptors located in the muscles and the joint-supporting ligaments (attitude). “There are specific nerve receptors for this form of perception termed "proprioceptors", just as there are specific receptors for pressure, light, temperature, sound, and other sensory experiences. Proprioceptors are sometimes known as adequate stimuli receptors. For example, TRPN, a member of the transient receptor potential family of ion channels, has been found to be responsible for proprioception in fruit flies, nematode worms, African clawed frogs, and zebrafish. PIEZO2, a nonselective cation channel, has been shown to underlie the mechanosensitive of proprioceptors in mice. The channel mediating human proprioceptive mechanosensation has yet to be discovered” [34].

“Proprioception of the head stems from the muscles innervated by the trigeminal nerve, where the GSA fibers pass without synapsing in the trigeminal ganglion (first-order sensory neuron), reaching the mesencephalic tract and the mesencephalic nucleus of trigeminal nerve” [29][34].

Temporary defect or impairment of proprioception might happen periodically throughout growth, mostly during adolescence. Growth that might also have impact on this would be large increases or drops in bodyweight/size due to fluctuations of fat (liposuction, rapid fat loss or gain) and/or muscle constitution (bodybuilding, anabolic steroids, catabolism/starvation). It can also appear in those that concern new levels of flexibility, stretching, and twist. A limb's being in a new range of motion never tested (or at least,

not for a long time since youth perhaps) can interrupt one's sense of location of that limb. Possible episodes involve unexpected feeling that feet or legs are missing from one's mental self-image; needing to look down at one's limbs to be sure they are still there; and falling down while walking, principally when attention is focused upon something other than the act of walking.

“Proprioception is occasionally impaired spontaneously, especially when one is tired. Similar effects can be felt during the hypnagogic state of consciousness, during the onset of sleep. One's body may feel too large or too small, or parts of the body may feel distorted in size. Similar effects can sometimes occur during epilepsy or migraine auras. These effects are presumed to arise from abnormal stimulation of the part of the parietal cortex of the brain involved with integrating information from different parts of the body” [29].

Proprioceptive misconception can also be inducted, such as the Pinocchio illusion. The proprioceptive sense is often unnoticed because people will adjust to a continuously stimulus as a result of the typical state of human adaptation. The effect is that proprioceptive sensory impressions disappear, even as a scent can disappear over time. One sensible advantage of this is that unobserved actions or sensation continue while an individual's attention can move to another concern. The Alexander Technique directs these unconscious components by transfer attention to them and active a replacement movement with concentrate on however it feels to move in the new way. People who have a limb amputated may still have a confused sense of that limb's existence on their body, known as phantom limb syndrome. Phantom sensations can occur as passive proprioceptive sensations of the limb's presence, or additional active sensations like perceived movement, pressure, pain, itching, or temperature. There are difference theories regarding the etiology of phantom limb sensations and experience. One is the theory of "proprioceptive memory", that argues that the brain retains a container of specific limb positions which when amputation there is a discord between the visual system, that really sees that the limb is missing, and the memory system which remembers the limb as a functioning part of the body. Phantom sensations and phantom pain may also develop after the removal of body parts other than the limbs, like when after amputation of the breast, extraction of a tooth (phantom tooth pain), or removal of an eye (phantom eye syndrome).

Proprioception is an element of the synesthesia. The synesthesia is a sensorial perception phenomenon within the stimulation of one sensory or cognitive route leads automatically, involuntary experiences in a second sensory or cognitive experience. Good proprioception allows us to write legibly, walk in a straight line, dance to the rhythm of the music and do well during physical activity. It is not balance, but it contributes to allow an animal to stabilize itself against environment perturbations.

It is commonly believed that proprioceptive signals convert joint angles. To localize a hand (i.e., to find out its position) with respect to the body for instance, the CNS needs to know the angles of all joints between that hand and the body and combine these angles with the known segment lengths

"Joint position matching" is a protocol for the measurement of proprioception, and joint position sense specifically, without the aid of visual or vestibular information. During such assignments, individuals are blindfolded while a joint is moved to a specific angle for a given time, returned to neutral, and the subjects are asked to replicate the specified angle. Measured by constant and absolute errors, capability to precisely identify joint angles over a series of conditions is the most accurate averages of determining proprioceptive acuity in isolation to determinate.

Recent investigations have shown that hand dominance, participant age, active versus passive matching, and presentation time of the angle can all affect performance on joint position matching tasks. Without a measuring instrument, it is difficult, if not impossible, to say if there is progress in its own sense. The first problem that scientists have to face is that of being able to measure and quantify proprioception. INSERM wanted to study proprioception in sensitive subjects such as the elderly or people who had a stroke. In fact, after stroke, various neurological disorders lead to motor disorder, balance disorders and even proprioceptive anesthesia.

Biomechanics of upper limbs

In order to perform a motion analysis, the upper limb is simplified into a rigid body link-segment model with joints that have a fixed center of rotation; although this is only an approximation to reality, in most cases it is sufficiently accurate for the purposes of the analysis. The upper limb is considered to have seven degrees of freedom, namely three at the shoulder (glenohumeral joint), two at the elbow and two at the wrist; the scapula and clavicle are each considered to have three degrees of freedom. The difficulty is to reduce the complex shoulder and arm geometry into a simple link model.

Following the principal axis of the rigid body link-segment model:

- **Clavicular axis:** The clavicle is assumed to run from the centre of the SC joint to the centre of the AC joint.
- **Glenohumeral (GH) joint:** The GH joint centre is assumed to lie at the geometric centre of the humeral head. In absolute values, the centre is located (depending on the study) at a mean distance of 37–45mm inferior, 6–14mm lateral and 0–8 mm anterior to the AC joint, although a large variability among individuals is apparent.
- **Scapular plane:** In a link-segment model, the contribution of the scapula lies between the AC joint and the GH joint. The plane of the scapula, while easy to comprehend conceptually for the relatively flat bone, has been described in many different ways when trying to quantify it. The most common description is the plane formed by joining AC, TS and AI.
- **Humeral axis:** The humeral axis has most often been defined from the glenohumeral joint centre to midway between the medial and lateral epicondyles at the elbow.
- **Elbow joint:** The elbow joint is considered to be a two-degree-of- freedom hinge joint, i.e. flexion/extension and pronation/ supination. The flexion/extension axis passes through the centre of the trochlea.

- **Carrying angle:** An angular offset exists at the elbow called the carrying angle. Conceptually the carrying angle is the angle between the ulna and the extension of the humerus, when the arm is in the anatomical position. It is typically between 5 and 15° for men and 10 and 25° for women. This angle occurs due to both a tilt in the humeral (flexion/extension) axis at the humeroulnar joint and an angulation of the ulna itself, showing large variations among individuals. The path taken by the forearm appears to be linear during flexion, at least up to 90° flexion. Although it is not usually reported in motion analysis studies, it is a necessary value when modelling the arm further. It has been handled differently by different researchers, including accommodating it by humeral rotation, assuming that it is due to a pure rotation of the humeroulnar axis or calculating it as a Euler rotation. Even those who study only the elbow have used three different definitions, which has been the source of considerable confusion. The carrying angle is not a degree of freedom but must be considered (due to the bony geometry) if the coordinate system is to be transformed between the humerus and the forearm. In this situation, it is probably best modelled as the second rotation in the elbow rotation sequence, following elbow flexion and preceding pronation/supination. The only active degrees of freedom that need to be reported, however, are flexion/extension and pronation/supination.
- **Wrist joint and hand axis:** The wrist is principally a two-degree-of-freedom joint including flexion/extension and radial/ulnar deviation although a minor amount of rotation is possible. The zero definition is with the third metacarpal bone aligned with the radius. The axis is forward of the mid-point between the radial and ulnar styloid processes, on the head of the capitate near the lunate/capitate articulation; the hand can be flexed back and forth to locate it. This axis is translated from the end of the pronation/ supination axis, but a simple hinge model is usually assumed.
- **Pronation/supination axis:** The pronation/supination axis passes from the capitulum on the humerus through the radial head to the distal end of the ulna; i.e. pronation/supination occurs by rotation of the radius about the ulna. Since the radial head is not midway between the epicondyles, however, there is a translational distance between the humeral axis and the forearm axis. Furthermore, the pronation/supination axis is 4–5° off the perpendicular to the flexion/extension

axis. Pronation/supination should be measured at the wrist where the radius rotates the most around the ulna. A link-segment model of the two-bone forearm is better represented by the ulna since this accurately defines elbow flexion/extension, and the carrying angle, but the pronation/supination axis then needs correction. Peterson treats the ulna and radius separately since a link-segment model with a single joint cannot represent pronation/supination accurately.

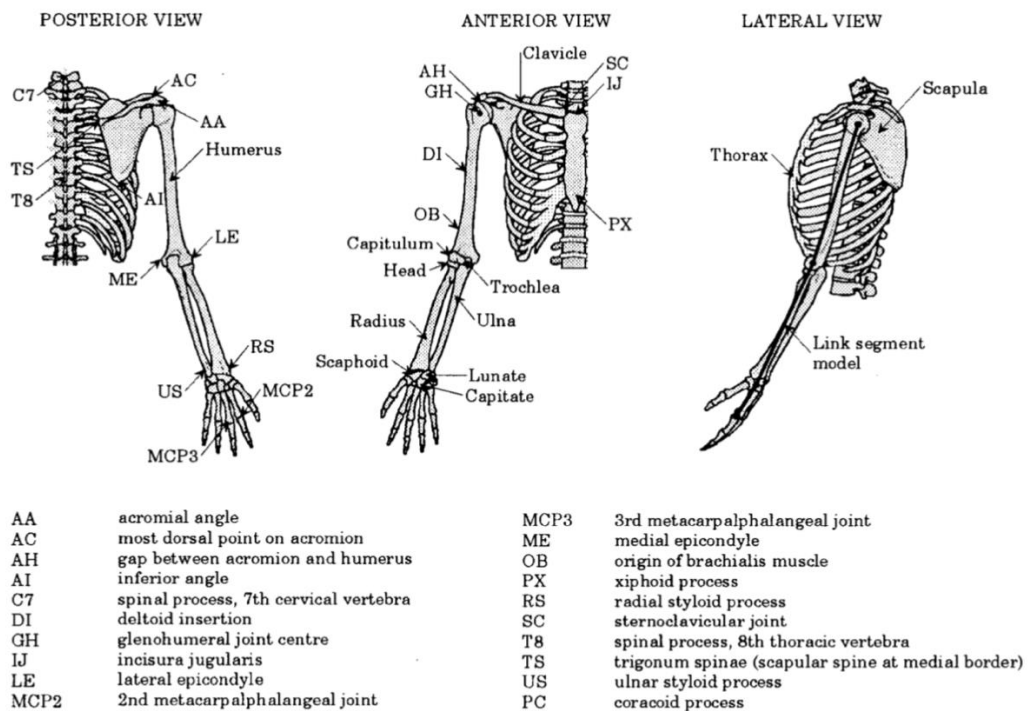


Fig.5 – Biomechanics axis

Control behavior of CNS

Humans exhibit a massive repertoire of motor behavior which permits us to interact with many alternative objects under a spread of various environments. From an engineering perspective the human neuromusculoskeletal system can be held as a robot, consisting of a linkage system (the skeleton) with motors (muscles), sensors (proprioceptors), and a control system (the CNS). The nerves and neurons are the links and junctions, which transport the data from the proprioceptors to the CNS and from the CNS to the muscles. Studies on our cognitive development reveal that the central nervous system (CNS) makes use of internal models in planning, controlling and learning of the mechanical behaviors. “In the subject area of control theory, an internal model is a process that simulates the response of the system in order to estimate the outcome of a system disturbance. The internal model principle was first articulated in 1976 by B. A. Francis and W. M. Wonham as an explicit formulation of the Conant and Ashby good regulator theorem. It stands in contrast to classical control, in that the classical feedback loop fails to explicitly model the controlled system (although the classical controller may contain an implicit model).

Internal models can be controlled through either feed-forward or feedback control. Feed-forward control computes its input into a system using only the current state and its model of the system. It does not use feedback, so it cannot correct for errors in its control. In feedback control, some of the output of the system can be feedback into the system’s input, and the system is then able to make adjustments or compensate for errors from its desired output” [33]. Two primary varieties of internal models have been proposed: *forward models* (FM) and *inverse models* (IM). In simulations, models can be combined together to solve more complex movement tasks.

Forward models capture the forward or causative relationship between inputs to the system. A forward dynamic model of the arm, for instance predicts the consecutive state (e.g. position and velocity) given the current state and motor command. The actual and foretold position of the body might differ due to noise introduced into the system by either internal (e.g. body sensors don’t seem optimal, sensory noise) or external (e.g. unpredictable forces from outside the body) sources. If the actual and predicted body positions contradict, the distinction can be fed back as an input into the entire system

additional in order that an adjusted set of motor commands can be figure out to make more accurate movements. Such models are planned to be employed in motor learning, state estimation and motor control [22][33].

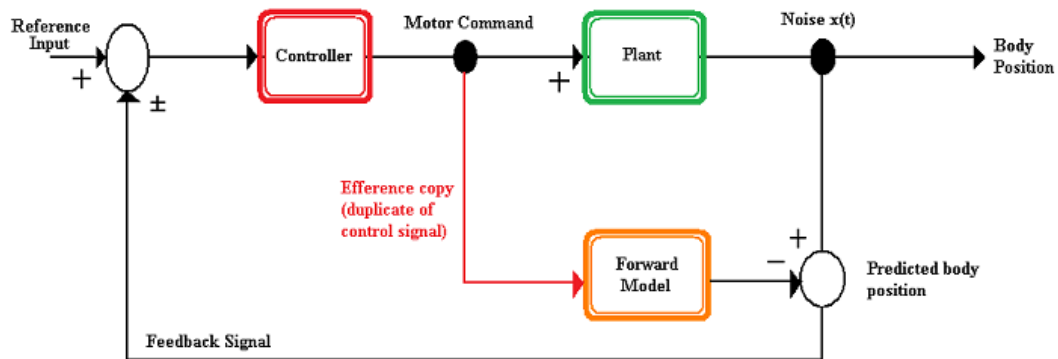


Fig.1 – Internal Forward Model

In contrast, inverse models use the required and actual position of the body as inputs to estimate the mandatory motor commands which might rework this position into the desired one. Inverse models are, therefore, well compatible to perform as controllers as they can supply the motor command necessary to achieve some desired state transition. Even control strategies, such as feedback control, which do not expressly invoke an inverse model, can be thought of as implicitly constructing an inverse model. It is in this area that we can work to understand better the control of Proprioception [22][33].

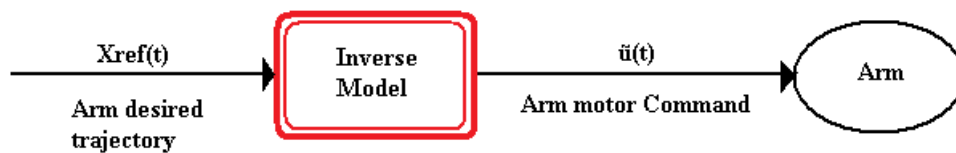


Fig.2 – Internal Inverse Model

Prototype

This thesis deals with postural control. Postural control is a specific case within human motion control. The human has to maintain a posture, i.e. an equilibrium position. During postural control two independent strategies contribute to stability and performance: (1) intrinsic properties of the muscles and (2) proprioceptive reflexes. With activation of a muscle not only the generated force increases, but also the viscoelasticity increases, i.e. the resistance to external disturbances. By coactivation of antagonistic muscles around a joint the joint remains in equilibrium and is less sensitive to disturbances. Proprioceptive reflexes from muscle spindles provide information about stretch and stretch velocity. This information is fed back to the motoneurons. A stretch after a perturbation results in selective activation and deactivation of the antagonistic muscles to restore the posture. Co-activation is very energy consuming as the muscles are constantly activated. Reflexes are energy efficient as the muscles are only activated in response to a present disturbance. Major drawback of reflexes is the time delay; reflexes are not instantaneous. It takes time to transport the signals over the nerves and to process the information. Also, the force build-up in a muscle takes time (activation dynamics). From control engineering it is known that the effectiveness of time delayed feedback is limited as oscillations and instability must be avoided. Smaller delay, i.e. faster response, gives larger stability margins and consequently can be more effective.

The upper limb can be sketched with 5 degrees of freedom indicated. Only three elements constitute an upper limb: the hand, the forearm and the arm. The elements are connected to each other by ball joints.

Nevertheless, in our study we consider that the hand and forearm act together, so they remain in the same position with respect to the other limbs during tests. The shoulder is fixed in the test, so the only main connection studied is that of the elbow. Another hypothesis therefore corresponds to precisely locating the center of rotation of the elbow in the upper limb. This center of rotation is considered at the intersection of the axes of the arm and forearm, ie approximately in the center of the elbow section.

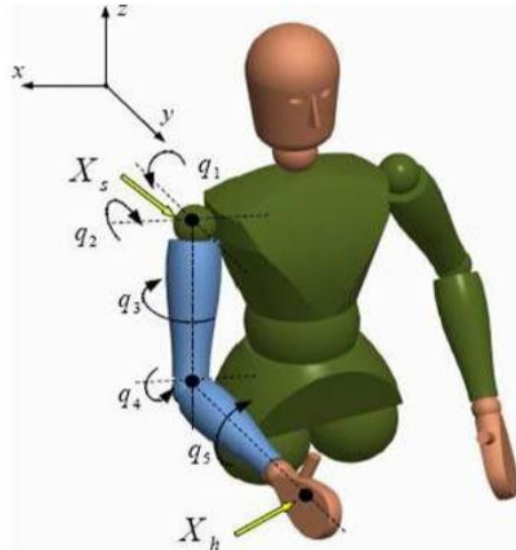


Fig.6 – Degrees of freedom

Default values

The subjects tested are of standard height and weight for men and women aged between 8 and 70 years. We therefore believe that the size and masses of each subject may vary, but to a reasonable extent to minimize the number of parameters on the test device.

The total weight of the limb and hand is considered between 2 and 4 kg, but a more precise indication can be issued using the Dempster table:

<i>Structure</i>	<i>% of total mass</i>	<i>Mass [kg]</i>	<i>Location of gravity Center</i>
Arm	2,7	2,54	Middle part of humerus
Forearm	1,6	1,72	Above the middle part of the forearm
Hand	0,6	0,64	Middle part of the 3rd metacarpal
Total	4,9	4,90	

<i>Anthropometric measurements</i>	<i>Man [cm]</i>	<i>Woman [cm]</i>	<i>Margin considered</i>
Shoulder width	44,5	40	25 – 45 cm
Forearm length, outstretched hand	47,5	42,5	20 – 40 cm
Height of the axis of rotation of the elbow	/	/	2 - 4,5 cm

Description of the project

The goal is to design a device to examine the proprioception of the limbs in subjects using multi-plane contralateral and ipsilateral tests (sagittal and horizontal plane).

During the experiments, the subject sits in front of the camera with his limbs attached to the support. His eyes are blindfolded to make him use only his arms as sensors. The experimenter stands next to the subject, ready to launch acquisitions.

The first contralateral test consists of passively bending the elbow of the subject's dominant limb to reach a certain angle. The subject must therefore reproduce the same angle with the other forearm. The proprioception will be qualified by measuring the difference between the two acquired angles. The second ipsilateral test is almost identical: the elbow of the subject's dominant limb is bent at an angle and then returned to its initial position. It is the same limb that has to perform this movement again after the initialization of the position.

The device must be able to integrate these two bending / extension tests of the forearm in the sagittal plane of the subject and in the horizontal plane, as shown in the examples a) and b) respectively present in the literature.

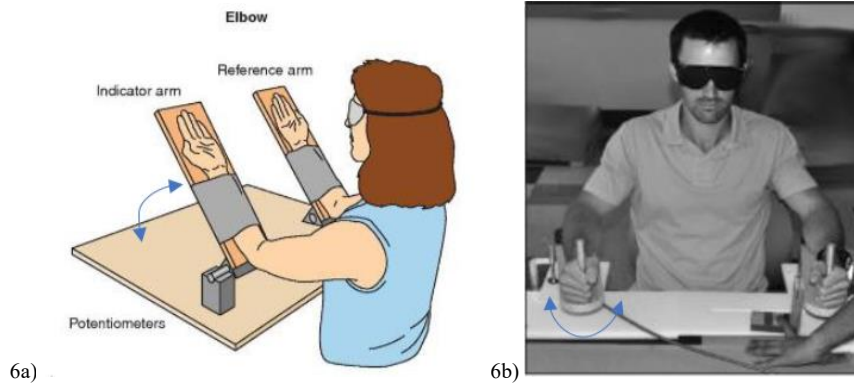


Fig.7 – Horizontal/Vertical test

Device specifications

The system must have 2 degrees of freedom: a rotation in the sagittal plane and a rotation in the horizontal plane. The rotations are independent, the movement is performed only on the sagittal plane or only on the horizontal plane, from the initial position. The movement is performed in the following places, followed by the same, it is not permeable, but it is an advantage, if it is feasible at the same cost. The movement can be controlled manually or via actuators.

The device must measure the angles of both rotations. The measurement is made between the initial position and the position to be measured in the system. The accuracy of the measurement must be at least 0.1° . The measurement must be stabilized. The methods of activation of the measurement must ideally be performed by the subject and must not disturb the position of the limb at the time of measurement.

In its initial position, the limb has the elbow bent at 30° in the sagittal plane (angle between the forearm and the axis of the arm) as shown in Figure 7a), at 0° in the horizontal plane, the forearm aligned with the axis of the arm in the horizontal plane as shown in Figure 7b).

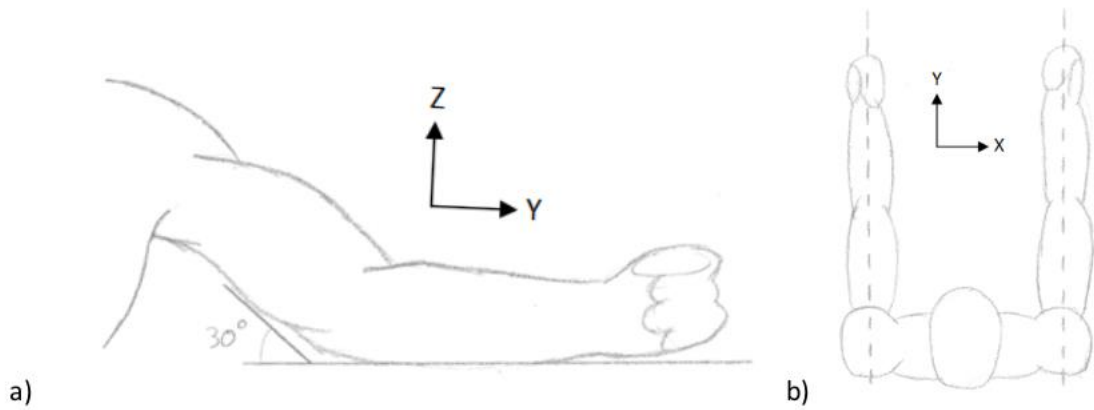


Fig.8 – Initial position of arms

The rotation in the sagittal plane must allow an amplitude ranging from 30° to 135° . Measurements will be made with angles of 50° and 70° (Figure 8a)).

The rotation in the horizontal plane must allow an amplitude ranging from -30° to $+30^\circ$. Measurements will be made with angles of -20° and $+20^\circ$ (Figure 8b)).

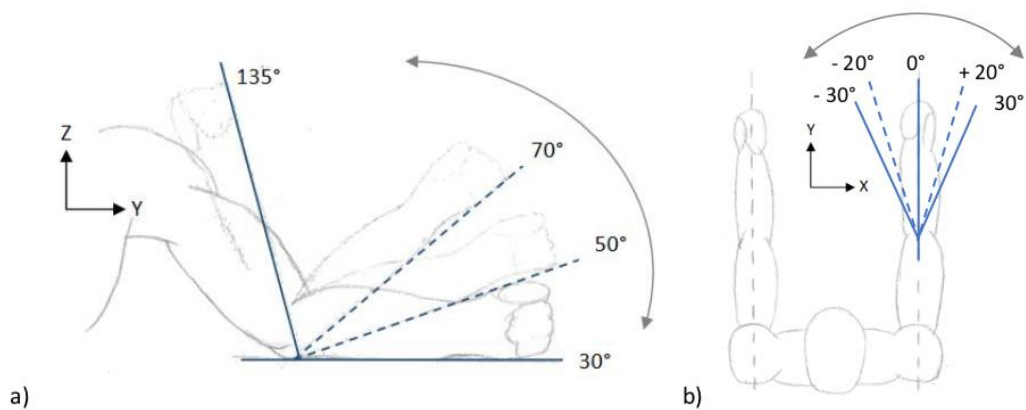


Fig.9 – Angles of rotations

The system must be symmetrical, the two parts can be used as a guide or follower, depending on the dominant limb of the subject.

The entire limb must be firmly attached to the system, the arm and forearm must be pressed against the system bracket to avoid distorting the angle measurement. The hand

must tighten a handle to remain oriented in the same way with respect to the forearm during the tests.

The distance between the two parts must be adjustable to respect the distance between the subject's shoulders. The hand must be able to slide on the support to allow movement. The height adjustment of the subject in relation to the camera can be performed outside the system or can be performed there.

The system, positioned on a table, must not move during use. Both parts must respect a certain alignment and parallelism to avoid having a measurement error due to the initial position.

The security of the subject must be guaranteed by a software and a mechanical stop system. The system must not move the subject's arm in a non-compliant manner that could cause dislocation or injury. Furthermore, a certain comfort must be guaranteed for the user, especially at the level of the elbow.

No evidence, on which the subject could rely, should disturb the proprioception. This can be caused by engine noise, machine vibrations or movement such as hand slipping on the support. It is therefore necessary to prevent any type of test of this type that could distort the proprioception test.

The subjects tested are standard height and weight for people aged 8 to 70 years. The weight of the forearm alone is considered between 2 and 4 kg. The additional weight that the arm must lift to reproduce the movement must be minimized. In fact, a weight added to the movement of the limb can create a positioning error.

First prototype

A first prototype was designed by the INSERM team and meets the desired primary needs but remains inconvenient and requires more functionality.

As can be seen in Figure 10, the first prototype could make only one movement in the sagittal plane. The equipment allows to fix the support of the arm at 20 ° or 40 ° and therefore to measure the angles when the subject is tested with an inclinometer. The device is not automated and the two parts of each arm are neither connected to each other nor fixed to the table. The comfort of the mechanical arm is quite rudimentary, but sufficient. The support parts are made of PVC and then glued or screwed together.

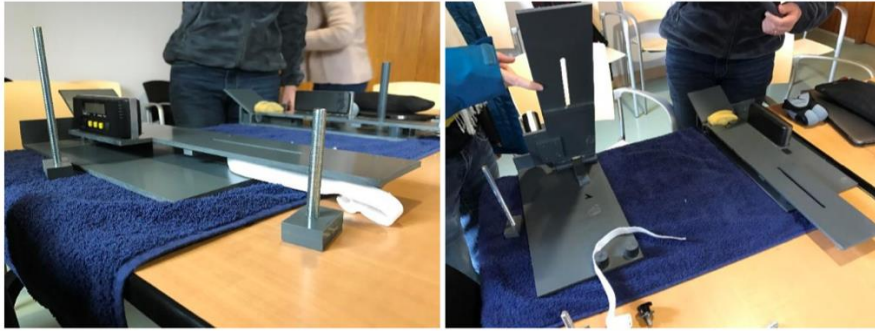


Fig 10 – First prototype

One of the first traces to improve is the position of the axis of rotation of the support: it is too far from the axis of rotation of the elbow and therefore creates a transverse movement of the hand on the support during the raising of the forearm. Thus, a slot in the support allows the hand to hold a handle that can move freely and follow the movement of the hand. Furthermore, the measured angles are read directly by the inclinometers until the arm stabilizes. This results in inaccurate measurements, even if the first tests showed only plausible results.

The general form of support should be maintained, but it has been said that it is not necessary to limit their creativity to find the best possible design.

State of the art and design ideas

Secondly, a scan of the existing solutions was performed. Very few devices are designed to measure the proprioception of the elbows, however many devices can be used to re-educate a patient's limb using a design close to our project.

For example, the Fisiotek device shown in Figure 11 can rehabilitate patients' elbows by working on their flexion and extension under different loads. The general shape of the device, including the separation between the arm support and the forearm support, which allows for better rotation, looks interesting. The idea of a cylindrical support that fits better with the shape of the arm also seemed relevant. However, such a support can give some sensory cues to the subject during the movement and can therefore disturb the results.



Fig.11 – Fisiotek device

It is also in the article by Fuentes and Bastian [*] that a camera very similar to the one imagined was presented: the KINARM (Figure 12: Photo of the KINARM camera, developed in Canada by the BKIN Technologies team, KINARM (Kinesiological Instrument for Normal and Altered Reaching Movement) allows the exercise of a subject's elbow in the horizontal plane. The design of the device with a metallic appearance showed us that it was necessary to design a device that was pleasant to see and handle for the subject. To the extreme, the camera should not be scary, as some subjects will be children or old people who might be reluctant to insert their arms into a "heavy" metal machine. Furthermore, as for KINARM, the device must be easily adjustable, without tools or special forces.

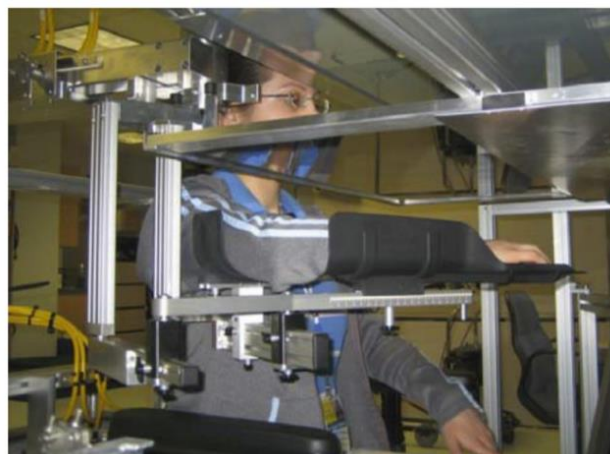


Fig.12 – KINARM camera

Finally, when looking for solutions to power the device, the cable solution was found. This point will be further investigated later. Figure 13 shows a diagram of the CaMaReS

device which should allow a gradual re-education of the patient's limb. Other devices also use this system, such as Rosati et. al. o Jin et. al. . The motors placed on a structure around the patient control the length of the cables connected to the patient's arm to move it into space. The idea of using cables to power a limb is very interesting because it is reassuring in the sense that it seems less harsh than the cylinders or the motors close to the patient. The use of this cable system in a medical context shows that it is a common process and therefore adapted to the device to be used.

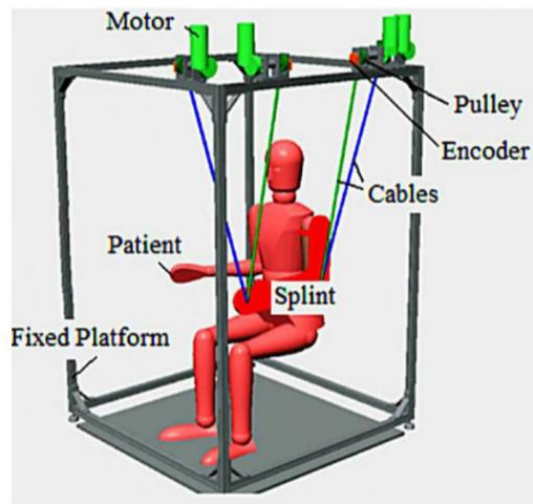


Fig.13 – CaMaReS device

Resolutions - Design and connections of the arm support

In order to rotate in the sagittal plane and in the horizontal plane, two degrees of freedom are required on the support. Different solutions are being studied.

The first two combine a horizontal pin that allows rotation in the sagittal plane and a vertical pin that allows rotation in the horizontal plane. Since the connections are in series, what differentiates the two solutions is the order of the solutions. The black part that represents the frame, the green the horizontal pin and the red the vertical pin, so for the first solution (Figure 14a): frame - rotation in the sagittal plane - rotation in the horizontal plane; for the second solution (Figure 14b): frame - rotation in the horizontal plane - rotation in the sagittal plane. Since the movements are carried out in the two planes in different ways, the order has no influence. This will have an influence if the two movements are combined without returning to the initial position, but this is not required

in the specifications. However, the second solution has the advantage of allowing the horizontal pin to be aligned with the axis of rotation of the elbow, unlike the first solution. The first two solutions offer links corresponding to the specifications. The third solution (Figure 14c) combines links that respect the kinematics of the human limb. The rotation in the sagittal plane is simple because it corresponds to the rotation of the elbow, so there is no difference for this rotation with respect to the first solutions which remain a horizontal pin. However, the movement becomes more complex due to the rotation in the horizontal plane. In fact, there is no axis of rotation of the elbow that allows this movement to be performed directly, it is a combination of the rotation of the elbow and the rotation of the arm on the shoulder. This solution, unlike the first ones, allows to combine the two rotations and therefore to create a more complex movement. This solution also prevents friction of the mechanical arm on the support during rotation in the horizontal plane. However, making the blue link is more complex because it has to be done around the arm.

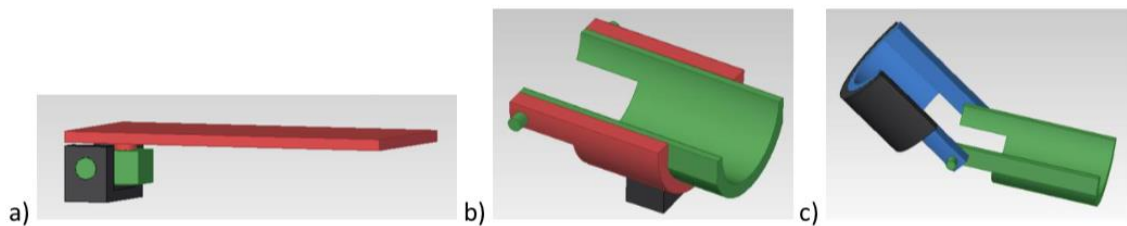


Fig.14 – Different solutions studied

The solution 3, a priori more interesting, proved to be too complex in the design. Since the combination of the two rotations was not required in the specifications, the choice of solution 2 was made at the end.

Motorization of the system

To start the support, it was designed to operate the connections directly.

The first solution is to operate the cardan shafts directly from the engines. However, defining a maximum weight of the forearm and hand of 4 kg and a maximum length of the forearm of 40 cm, assuming that the center of gravity is at the center of the forearm,

a minimum torque of 8 Nm is therefore necessary to lift the forearm in the sagittal plane. This requires mounting a large engine and weight on the arm support.

A second solution was to place a cylinder between the arm and the forearm. However, a cylinder with sufficient power and travel is too large and expensive.

This system can be replaced by a cylinder with a rope that connects the arm and the forearm plates. Thanks to an engine that rolls the rope, the forearm can be raised.

A final solution is a connecting rod system. A connecting rod is in a fixed pivot connection on the forearm and in connection to a pin that slides along the arm. The length of the connecting rod that is fixed, when moving along the arm, the elbow bends or opens. The sliding can be performed by pulley-belt or ball screw (Figure 15). The ball screw reduces the engine torque required.

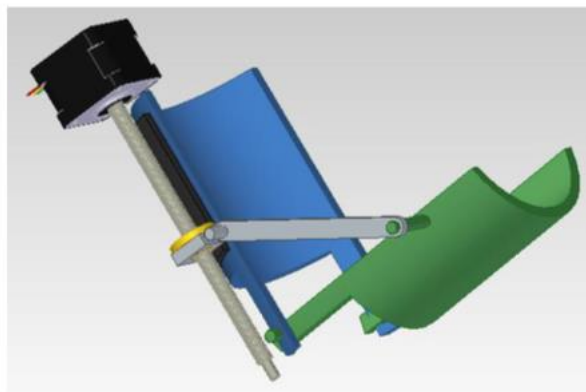


Fig.15 – Final solution

However, all these solutions are integrated into the support, which adds weight and support to the support and reduces the security of the subject. The choice is therefore to extract the motor from the support and simply control it by the handle. For this, the cables connected to the handle control the movement. Thanks to the motors that wrap the cables, it is possible to position the handle in the space provided by the colleague of the cables instruments.

Final solution

The machine is equipped with two "support" groups (Figure 16b), one for each limb. The subject places his limbs on this support, has different settings to adapt to the morphology of each person. This support allows two distinct rotations: rotation in the horizontal plane and rotation in the sagittal plane. The movement of the mechanical arm is controlled by a system of cables connected to the tip of the lancet. The three cables connected to each arm are driven by motors that wrap or unroll the cables. The supports, motors and pulleys are placed in a cage of 0.9 x 0.7 x 0.6 m (Figure 16a).

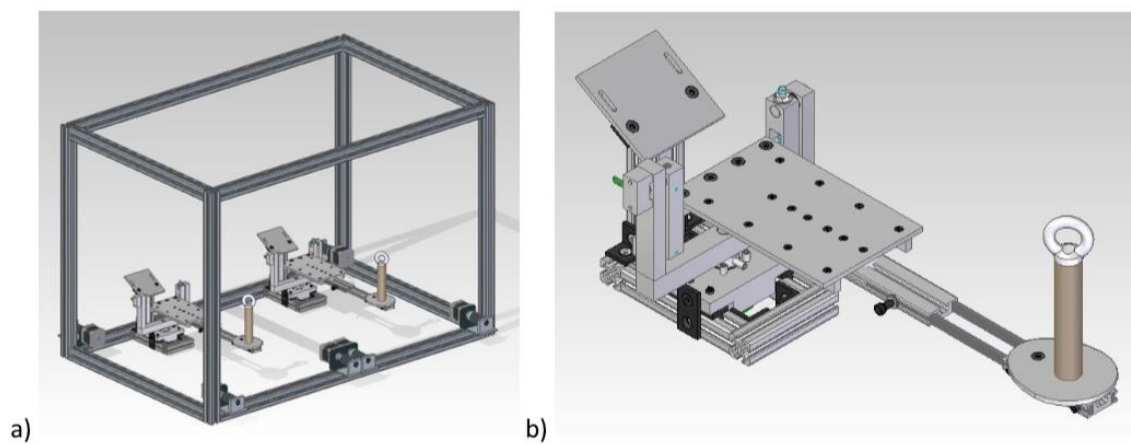


Fig.16 – Cage and Supports

The subject places the limb on the support with a plate under the arm tilted 30 ° from the horizontal, a plate under the forearm and a plate under the hand with a handle.

The plate under the arm is fixed and guarantees the initial position of the arm at 30 °, being the forearm plate horizontal.

The subject's arm is held on the support by a strap on the arm plate and on the handle.

Adjustments

For each subject it must be possible to adjust the length of the forearm, ie the position of the handle, the height of the axis of rotation of the elbow, as well as the distance between the shoulders.

The length of the forearm must be adjustable between 20 (Figure 17a) and 40cm (Figure 17b) from the elbow to the handle. This adjustment is carried out using a telescopic support with two slides.

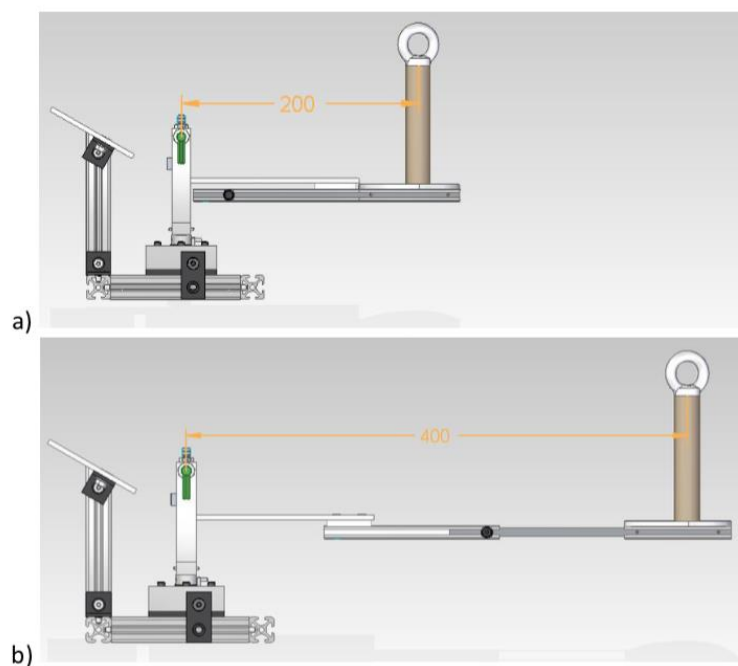


Fig.17 – Possible adjustments

The forearm support consists of a sheet, an aluminum profile and two rectangular steel bars. The bending of the bracket below the maximum weight must be minimized to avoid angular measurement errors. At the sheet level, the maximum deformation is calculated based on the following section:

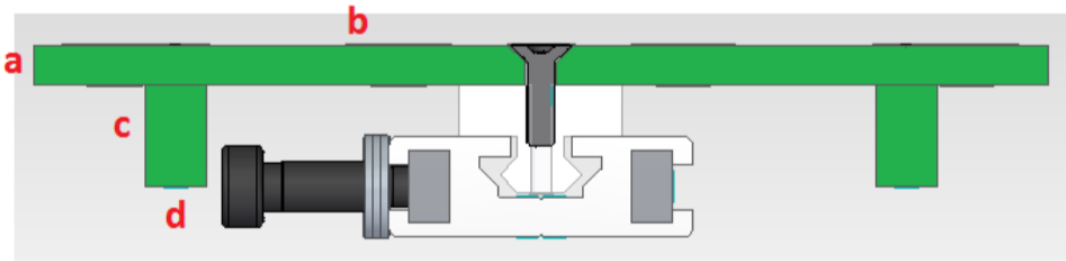


Figure 14 : Section de la tôle (en vert) support de l'avant-bras

Moment quadratique :

$$I = \frac{ba^3}{12} + 2 \times \left(\frac{dc^3}{12} + cd \times \left(\frac{a+c}{2} \right)^2 \right) = \frac{100 \times 4^3}{12} + 2 \times \left(\frac{10 \times 6^3}{12} + 10 \times 6 \times 7^2 \right) = 7413 \text{ mm}^4$$

Flèche :

$$\delta(L) = \frac{PL^3}{3EI} = \frac{40 \times 145^3}{3 \times 74000 \times 7413} = 0,075 \text{ mm}$$

In this way the arrow is small enough not to interfere with the measurements.

The height of the axis of rotation of the elbow is adjustable between 2 cm and 4.5 cm.

It must be adjusted in relation to the forearm and arm plates, so there are two adjustments to be made. The first is done by vertically moving the forearm plate with a screw. The second for horizontal translation of the forearm on the profile (Figure 18). The distance between the shoulders can be adjusted between 25 and 45 cm. The support of each arm runs through a bearing on the profile of the cage.

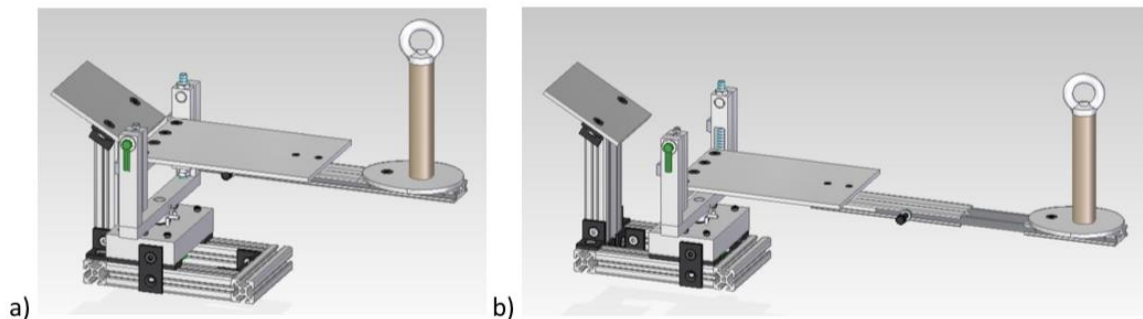


Fig.18 – Adjustments

Rotations

The rotation in the horizontal plane (Figure 19a) occurs in a range between 30° and -30° . The rotation in the horizontal plane (Figure 19a) takes place in a range between 30° and -30° . Rotation takes place between the vertical shaft and the support block using plain bearings. The pins are used as stops at the amplitude limits (Figure 19b).

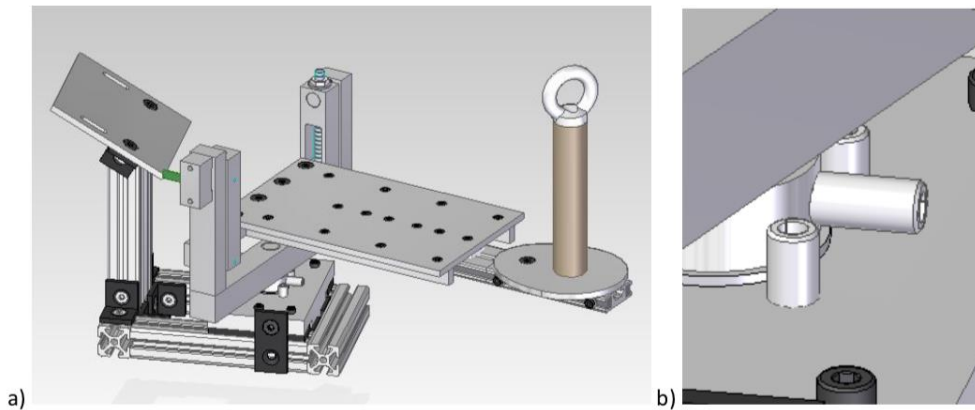


Fig.19 – Rotations

An absolute magnetic sensor fixed under the support block allows to measure the rotation angle (Figure 20). The sensor consists of two parts: the first part is the card fixed on the block of the hole that remains stationary, the second part is the magnet placed on the rotating shaft. The card detects the rotation angle of the Hall effect magnet.

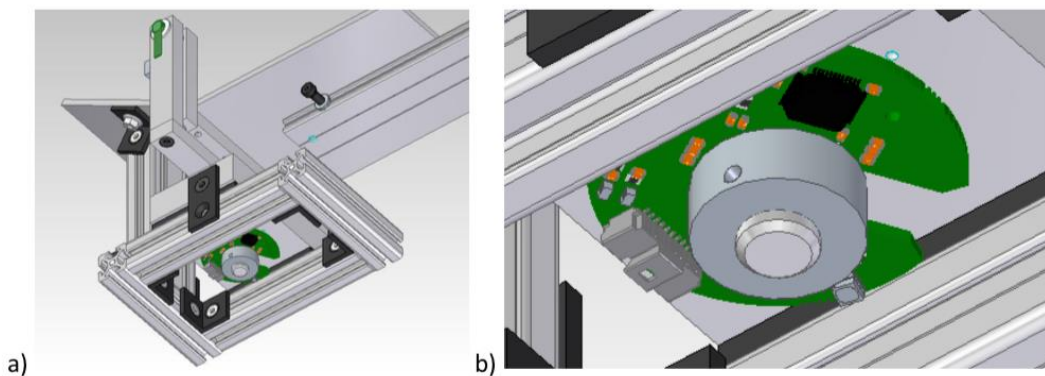


Fig.20 – Magnetic Sensor

The rotation in the sagittal plane (Figure 21) occurs in a range between 30 ° and 135 ° according to the specifications. In the initial position, a stop locks the forearm plate horizontally, ie at 30 ° of flexion, thus limiting the extension of the mechanical arm and thus ensuring the safety of the subject.

A sensor positioned on the fixed part measures the rotation by means of a magnet that moves with the shaft.

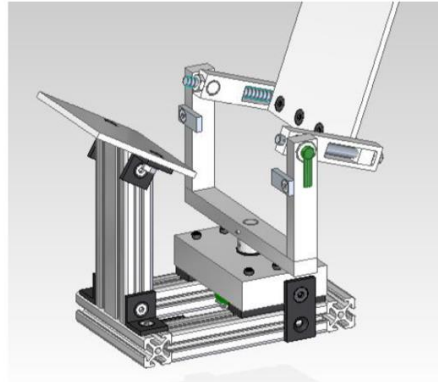


Fig.21 – Rotation in the sagittal plane

Cable control

The support is set in motion by the end of the handle to which the cables are connected. Each cable rises to a pulley fixed on the upper profiles. The pulleys rotate around their vertical diameter, which allows the cable to be directed towards the moving handle. The pulley returns the cable to the motor, fixed on the lower profiles, which rotates a winch on which the cable is wound (Figure 22).

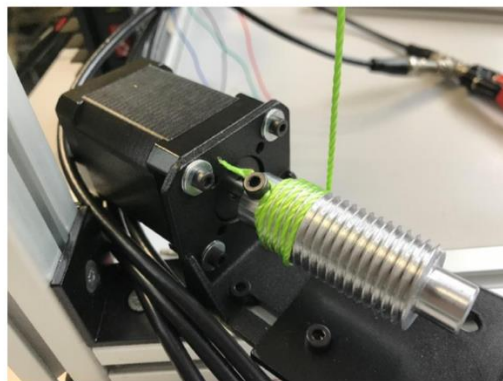


Fig.22 – Pulley with cables wound

Since the cables are stretched by the weight of the limb, three cables allow to impose the position in the space of the handle, knowing the length of each cable unwound. In this way, seen from above, one reaches the space delimited by pulleys. Three cables are therefore sufficient to obtain the three degrees of freedom necessary to move in space but limit the space that can be reached to a triangle. To have a space that can be reached seen from the top, the choice is made to have four cables, but operated by just three motors. The last two cables are actually just one, hanging on one side of the upper profile, then sliding into the handle ring and returning to the pulley and the engine.

Prototype production

The manufacture of the raw prototype, without robotics, was carried out by laboratory technician Hugues DORGERON. He took care of the preparation of the processing operations as a method department and of the processing of the pieces. The assembly of the parts was done in collaboration between him and us, because we knew the device better.

The total weight of the device is estimated at 18 kg. The support group of a single arm weighs 1.9 kg. It is important to emphasize that the weight of the support to be lifted, which had to be reduced to a minimum in order not to require too much effort by the subject, is 700 g.

The parts used are generally aluminum or an equivalent alloy. The good resistance of this material combined with its low weight perfectly corresponds to this type of device. Furthermore, their processing causes less damage to the tools. Some specific parts are made of other materials, such as the PVC handle or polymer sliding bearings.

Details of each part ordered are available in an attachment table 1. This table describes in detail the usefulness of each part, its material, its supplier and a link to the page of the supplier part.

Pièce	Nb pièces	Nb E/S	Description
MOTEURS	6	2	Alimentation moteurs 12 V ou 24 V – 2.1 A
	6	4	Connectique moteurs (déjà fournie)
	6	4	Sens de rotation (signe) et pulse (signal)
CAPTEURS	2	4	Capteurs sagittal en entrée
	2	2	Capteurs horizontal en entrée
	2	2	Alimentation sagittal 5 V (ou 3.3 V) – 26 mA
	2	2	Alimentation horizontal 4 à 6 V – 26 mA
BILAN	6 entrées (doubles) 12 sorties (doubles) 10 alimentations (doubles)		

Table 1 – Summary of the inputs and outputs of the device.

Fournisseurs	Types de pièces	Prix
RadioSpare	Fils électriques (câbles BNC)	126.60 €
Leroy Merlin	Câbles et visserie	11.57 €
Michaud Chailly	Paliers lisses	19.03 €
Motedis	Profilés et visserie	356.86 €
Portalet	Poulies	117.70 €
RLS	Capteurs	328.60 €
SAGE (INSA)	Visserie et bruts	129.88 €
Stepperonline	Moteurs et drivers	333.90 €
Systéal	Profilés et visserie	39.16 €
TOTAL		1 336.70 €
TOTAL (avec fils électriques)		1 463.30 €

Table 2– Spend Review by Supplier

Rotation sensors

The rotation sensors are the most important parts of the device: they provide the result of each experiment. These results will be useful in INSERM. It is therefore necessary to have precise parts to obtain a realistic result, and light parts so as not to hinder the subject's movements.

To meet these conditions, magnetic sensors have been used. Their advantages are good accuracy, high resolution (0.01°), small size and non-contact measurement.

We therefore ordered two different sensors for both rotations from the supplier RLS:

- 2 "Orbis™ absolute rotary encoder" for horizontal rotation
- 2 " RM08 super small non-contact rotary encoder, RM08I " for sagittal rotation

However, these two sensors have an accuracy indicated by the supplier of $\pm 0.3^\circ$. This does not correspond in the first place to the specifications set by INSERM, which required an accuracy of 0.1° . In relation to the possible confusion between the resolution (number of digits) and the accuracy (difference with the truth) of the INSERM, we found no rotation sensors of this accuracy. These first RL" sensors were installed on the machine, so it will be necessary to decide whether to use more precise sensors later.

The sensor in the sagittal plane, supplied with 5V, sends an incremental output. A change in the state of the A or B signal increases the angular position by a "count per revolution", $360/4096^\circ$ in our case. Signals A and B are out of phase by a quarter of a period. The direction of phase shift indicates the direction of rotation. The Z signal sends a pulse when the sensor has completed a full revolution.

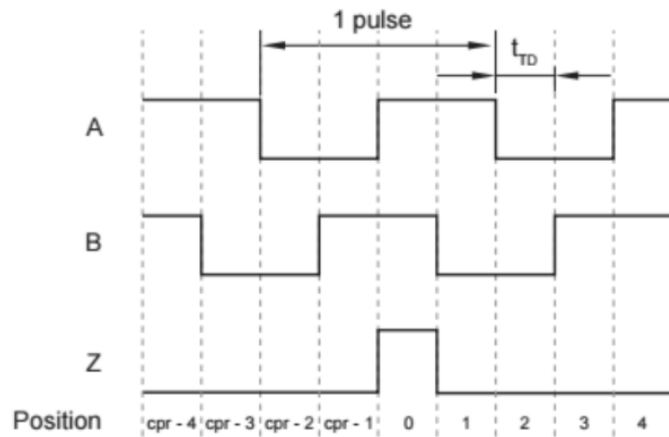


Fig.23 – Signal A,B and Z

The direction of the phase shift induces a different sequence of states. So for $[A(n-1) = 0$ and $B(n) = 0]$ or $[A(n-1) = 1$ and $B(n) = 1]$, we will have a first direction of rotation, otherwise the other direction.

The sensor in the horizontal plane sends a PWM (Pulse Width Modulation) signal. This signal therefore has a constant time period but a duty cycle that varies according to the angular position.

A minimum high state corresponds to an angle of about 360° , a maximum high state at an angle of 0° (Figure 21). In the middle, the width of the high state is proportional to the angle, so it is easily found thanks to the following formula:

Since the signal period is $8192 \mu\text{s}$, a minimum acquisition frequency of 440 kHz is required to have an accuracy of 0.1° .

A board made by the technician allows this signal to be translated into an analog signal. The signal value indicates an angular position.

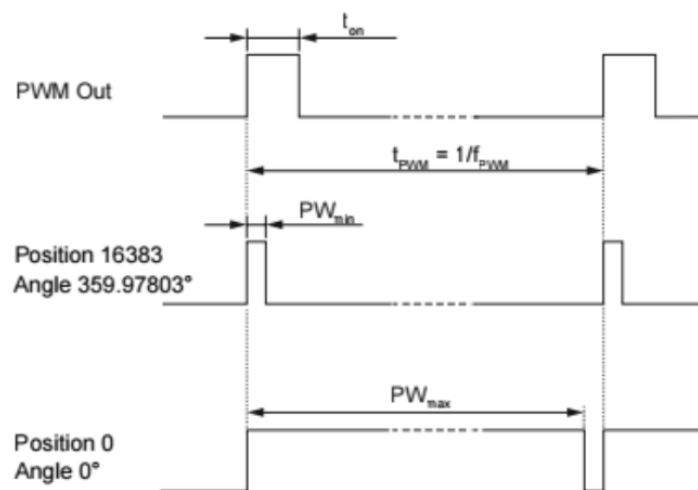


Fig.24 – PWM (Pulse Width Modulation) signal

A minimum high state corresponds to an angle of about 360° , a maximum high state at an angle of 0° (Figure 24). In the middle, the width of the high state is proportional to the angle, so it is easily found thanks to the following formula:

$$Angle (^{\circ}) = \frac{(t_{on} - PW_{min}) * 360}{PW_{max} - PW_{min}} = \frac{(t_{on}(\mu s) - 0.5) * 360}{8191.5 - 0.5}$$

Since the signal period is 8192 μs , a minimum acquisition frequency of 440 kHz is required to have an accuracy of 0.1 $^{\circ}$.

A board made by the technician allows this signal to be translated into an analog signal. The signal value indicates an angular position.

The motors

After several camera projects, we chose to motorize the support of the subject's limb with cables. The motors rotate a threaded rod that wraps or unwinds the cables to manage their length to the handle of the support.

The choice is made for stepper motors, which allow good positioning accuracy and open loop control.

The calculations on Matlab allow to obtain the torque as a function of the trajectory, the speed and weight of the handle, the torque as a function of the speed of rotation of each motor. This provides the most critical use case of the engine (Figure 25). The engine chosen is the smallest that allows to reach this most critical case, as shown by its operating curve (Figure 26).

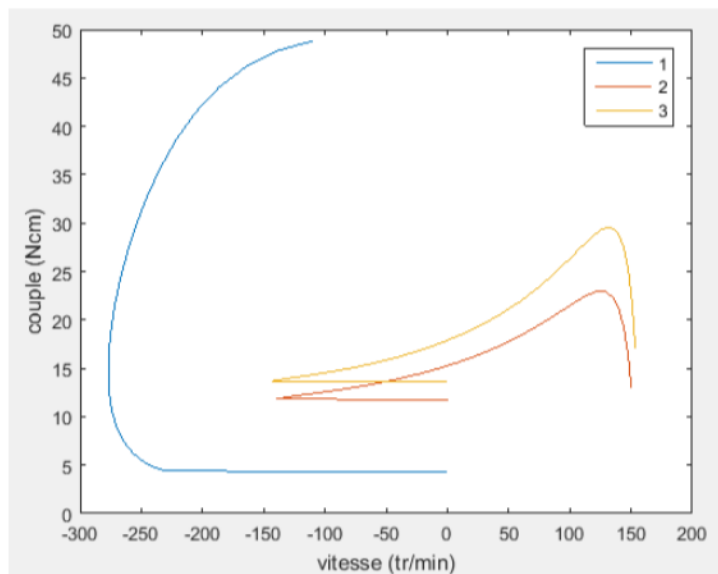


Fig.25 – Torque as a function of the trajectory

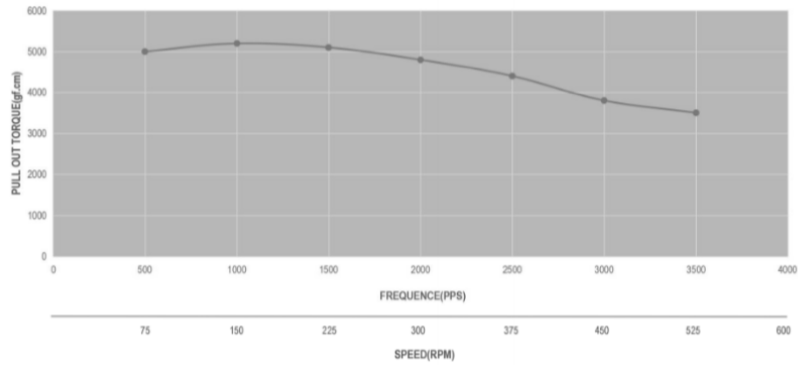


Fig.26 – Critical case

This is a standard NEMA 17 size motor, supply voltage 12-24V, rated current 2.1A with 200 steps per revolution, ordered from Stepperonline reference 17HS24-2104S.

A driver (Bipolar Stepper Motor Driver Max 3A Current 128 High Subdivision ST-7128) adapted to the selected motor allows control of the motor. Connections to the driver are made as follows:

- DC+/DC- : Power supply 12-24V
 - A+/A-/B+/B+/B+/B+/B-: two wires from one motor coil on A, two wires from the other coil on B
 - PUL+/PUL- : 0-5V square signal, one pulse turns the motor by one step.
 - DIR+/DIR- : square signal of 0-5V, direction of rotation of the motor, rotates in a 0V direction and in
- on the other side at 5V
- ENA+/ENA-: to be left disconnected

A code per switch allows you to choose the intensity supplied to the motor from 0.6 to 3.0A, and the microstep mode from full step to 1/128 step. Reducing the pitch obviously increases accuracy, but it also reduces the vibrations in the motor, which are very important for a whole step. However, this has the disadvantage of reducing the torque provided by the motor.



Fig.27 – Bipolar Stepper Motor Driver

In this way the motor can be rotated by choosing the direction and speed. The first is set by sending a high or low state to the DIR input, the second by varying the frequency of the square PUL signal.

Trajectory calculation

The objective of this part is to set the arm support in motion following a circular trajectory of the center of the elbow position.

The origin of the marker (Oxyz) is on the top of the cage as shown in the figure.

25. The positions of the pulleys in (xyz) are measured on the device.

The initial position of the bracket for each start of the trajectory is horizontal (zero sagittal plane angle) and perpendicular to the shoulders (zero horizontal plane angle). The position of the handle in the space at the beginning is known by an initialization phase of the device. The x position of the elbow is equal to that of the handle (zero horizontal plane angle), the z position is constant on the device and the z position is measured on the device and inserted on the interface by the user.

The trajectory of the handle tip is calculated from: the chosen plane, the chosen angle, the elbow position, the forearm length and the desired speed of rotation. This gives in equation:

$$x = x_C + R \sin(\omega n f) \sin \alpha$$

$$y = y_C + R \cos(\omega n f)$$

$$z = z_C + R \sin(\omega n f) \cos \alpha$$

with

- (x,y,z) : handle coordinates at time n*f (mm)
- (xC,yC,zC) : elbow coordinates (mm)
- R: forearm length (distance between elbow axis of rotation and handle) (mm)
- ω : forearm rotation speed (rad/s)
- f : time of a calculation phase (s)
- n : number of calculation steps since the beginning of the trajectory
- α : angle of inclination of the trajectory plane with respect to the plane (yz)

The spatial position of the handle is first calculated in the plane (Oyz) where the handle follows a circular trajectory of centre C (the elbow) (Figure 27a), then projected on an inclined plane of α rad with respect to the plane (Oyz) around C (Figure 27b). So to have a rotation of the arm in the sagittal plane it is necessary to choose $\alpha=0$ and for a rotation in the horizontal plane $\alpha=\pi/2$.

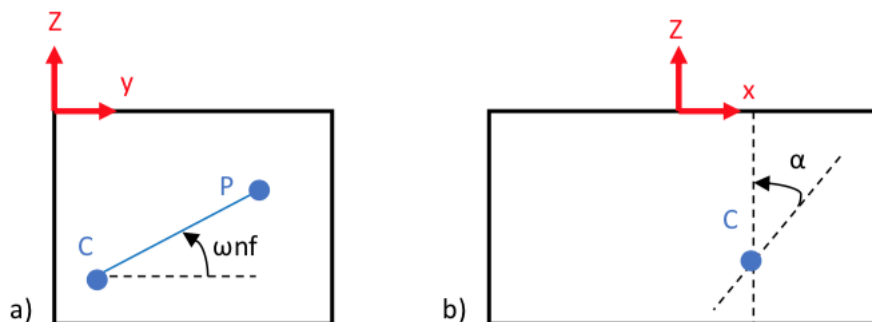


Fig.27 – Spatial position

Simulink Programming (MATLAB)

To function properly, the electronic parts of the device must be connected together. The logical connections between each input and output of the device can be managed by the MATLAB software via "Simulink". The created model thus connects the three previous parts.

The Simulink model called `piloting.mdl`, illustrated in the following page, has several parameters

from the beginning. Some of them can be modified by the user from the interface:

- Plane: 0 = sagittal; 1 = horizontal
- Covered corner
- Test: 0 = Ipsilateral; 1 = Controlateral
- Dominant arm: 0 = right; 1 = left
- Y position of the elbow
- Maintenance time

Some parameters are constant and cannot be changed by the user interface:

- Rotation speed: $\pi/6$ rad/s
- Time of a calculation phase
- Elbow Z position
- Motor pitch angle: 1.8° .
- Microstep: 1/8

The program also receives the input signals from the four sensors, which are processed to recall the angular values.

The program outputs a signal for the direction of rotation and a square signal to the motors to turn the motor.

The program will allow, according to the parameters chosen by the user via the interface and the option

to determine the frequency of the signal to be sent to the motors and the direction of rotation.

The "Lengths" subsystem allows to recalculate in real time the length of the unwound cables according to the speed and direction of rotation of the motors. It also allows calibration of the cables (Appendix *).

The 'Winding - Unwinding' subsystem makes it possible to control each motor in one direction or the other at constant speed (Appendix 1).

The 'Initialisation' subsystem makes it possible to pull the cables to a support position of 0° in the horizontal plane and 0° in the sagittal plane (Appendix 1).

The 'Trajectory' subsystem allows the engines to be controlled to follow the test mode and trajectory chosen according to the parameters entered via the interface. It calculates the position of the handle in space at all times according to the trajectory seen above. From these positions the length of the cables unwound at all times is deduced. The difference in cable length between two moments makes it possible to deduce the speed of rotation of the motors at all times (Appendix 1).

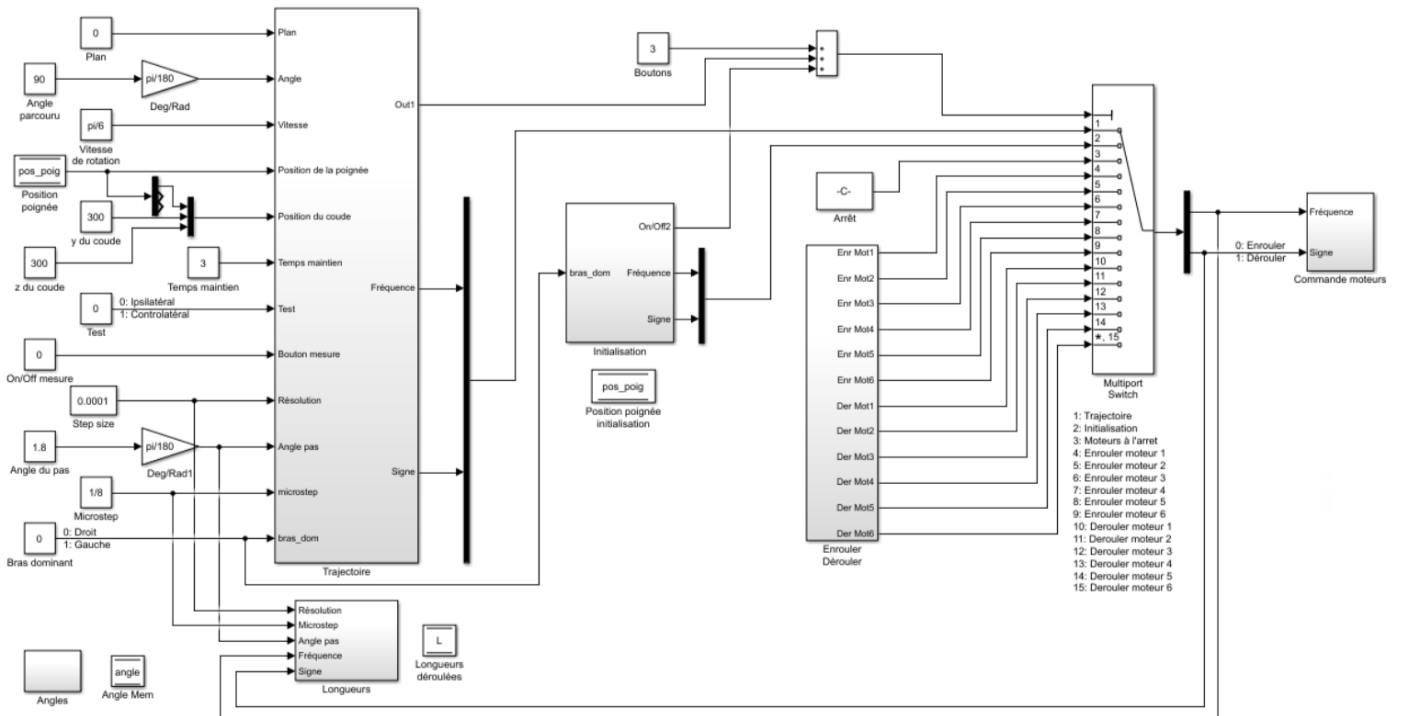


Fig.28– Simulink model of the prototype

The controls

Several tests must be performed to validate the use of the device, especially since a human subject will introduce his or her limbs into the device. However, the regulations in force regarding the use of this machine are not known. The INSERM team that is used to these devices is aware of this.

For the moment, we have performed some basic tests on the physical capabilities of the device:

- The rigidity of the structure seems sufficient. The structure can be easily moved by two people thanks to the handles and passes through classic sized doors.
- The movements of the subject's limbs do not seem to be hindered by parts, especially the motors. The only annoyance appears in the case of a contralateral test for a rotation

in the horizontal plane with an angle of -20° : the two hands touch each other if the shoulders (and therefore the arms) of the subject are not too far apart.

- The slider connection for shoulder width is correct: everything is rigid, well sized and repairable, even if the slider bearings are not "slippery" enough in the profile.

- The winding system seems to work correctly with polypropylene wires. The wire adapts well to the winch groove during winding. The wires remain tight in general. When the carabiner is loosened, the wire remains taut behind the pulley and does not unroll the winch. We don't have to give it too much play.

- For a tone of $1/8$ of a full pitch, the vibrations of the motor are reduced but remain substantial and propagate in the structure. Even running engines make a loud noise. It is necessary to find a solution for these problems.

Subsequently, many tests must be carried out to make sure that the device does not affect the measurement. The specifications specified that it required a minimum of sensory signals, both tactile and audible, in order not to guide the subjects. These aspects must be checked once the unit is fully assembled.

Zettlex IncOder

During the first meeting with Salam Bahmad, PhD student at INSERM, we have discussed about what are the possible implementations to make on the prototype.

At first time, it was necessary to do a check of the machine to verify what are the problems and then we established the main objectives of the work:

1. Find a better Encoder, with improved accuracy;
2. Implementation of other sensors (like accelerometers) to obtain more precise data about the position of the limb;
3. Review the design of pieces to block and change mobility of the mechanical arm;
4. Design new components to improve the control part to follow the movement of the arm when the subject is active;
5. Improve the overall ergonomics of the prototype;
6. Improve overall safety for both the subject and the operator;
7. Design ideally how to obtain a new diagonal trajectory for the test.

The first point elaborated followed the rapport on the possible encoders that could replace the “RM08I super small non-contact rotary encoder for the sagittal rotation” with another one with a better accuracy but, at the same time, not much bigger.

In general, the system for measuring the angle of rotation is composed of a mechanical interface for coupling to the application, from a disk (or other reading source), from electronic sensors, and from an electronic interface. In the case of incremental systems, the number of divisions (notches) of the disk is generally defined as the number of pulses.

An incremental system transforms a constant rotation of the motor shaft into a periodic signal. The frequency depends on the resolution (number of notches) of the disk. In the case of incremental encoders, there is no a priori absolute reference position of the measurement signal. An additional reference signal (zero pulse) can be used to uniquely define the initial position.

The mechanical interface is equipped with an axis that transfers the rotary movement to the rotor, of a flange, intended for mechanical coupling and which can be of the fixed type, square or servo, and of a "case" or the casing of the encoder. Both male shaft systems and hollow and / or through shaft systems are available.

The main features that define the mechanical system are:

- the maximum number of revolutions per minute, or the maximum rotation speed;
- the permissible axial / radial load on the shaft, ie the highest continuous or alternate force that can be applied to the shaft without exceeding the specified error limits or without impair bearing functionality.

The electronic interface is used both for the encoder power supply and for data transmission between the encoder and the external data processing system (PLC, pulse counter, speed and angle indicators). The electronic circuit can also process optional data such as diagnostic signals and information relating to position, speed, cams, the location of the rotor as feedback for the position control loop and switching of the motor phases.

Incremental encoders normally use a bar code composed of light / dark fields of equal width. For a relative movement of the optical disk with respect to the detection system (usually a phototransistor in encoders with optical technology) the acquisition system will receive a certain amount of optical pulses which will convert into electrical signals (channels). Staggering the light-sensitive surfaces of the detection system, the so-called scale increments are scanned twice and generate two electrical signals with a spacing of $\pi / 2$ corresponding to 90 degrees (a quarter of a period). It is thus possible to recognize the direction of rotation or the movement of the graduated scale with respect to the detection system. It is also possible to generate sinusoidal signals, which can then be digitized or interpolated, to obtain a higher resolution. Counting the sinusoidal signal passages from zero or the period fractions during interpolation the relative displacement is measured.

Since, with incremental measurement systems only the relative movement is determined and not the absolute position, in most cases a reference notch is applied on the incremental scale. Once this mark is exceeded, a reference signal is generated at the output, the so-

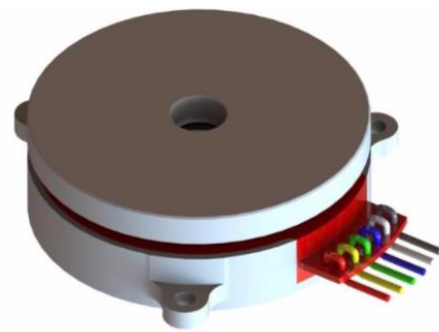
called zero pulse. This value is associated with a certain absolute position or a certain angular value.

One of the best encoders found on commerce is Zettlex IncOder: this is non-contact device for precise angle measurement. They use an inductive technique, similar to that used by electrical transformers.

The magnetic reluctance system is based on the measurement of changes in the resistance of the magnetic circuit caused by the passage of the teeth of the wheel set on the motor shaft. The magnetic band system uses a magnetic sensor that detects the field coming from a drum covered with a surface material for recordings on which the position signals have been engraved.

Fig.29 – Zettlex Incoder

It has two main parts each shaped like a flat ring: a Stator and a Rotor. The Stator is powered and measures the angular position of the passive Rotor. A big bore and low axial height allow easy integration with through-shafts, slip-rings, direct drive motors, optical-fibres, pipes or cables.



IncOders make it easy to achieve high precision, high reliability angle measurement as required ($\pm 0,1^\circ$).

All the electronics receive power and output a signal. The output signal shows the position of the Rotor relative to the Stator. Devices with absolute digital outputs, such as SSI, SPI etc., are truly absolute which means that they need no motion at power up to determine position. IncOders are designed respecting ISO-9001.

It's necessary to try if the new outputs digital could work with the rest of the system without any others modifications.

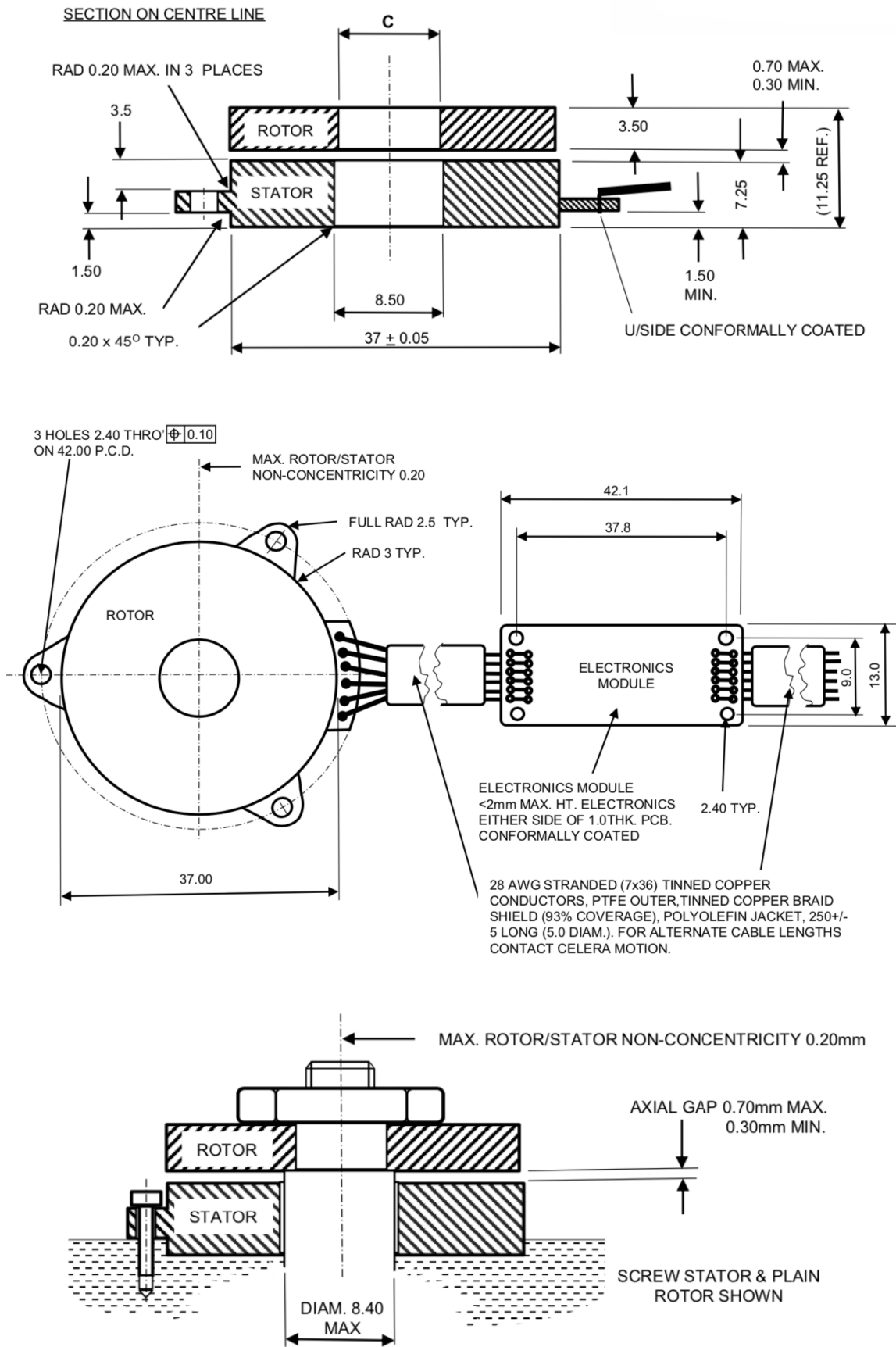


Fig.30 – Technical drawings

Measurement, Electrical, Environmental & Material Data for 37mm IncOder		
Measurement		
Measurement	Absolute over 360°. Note this is true absolute - no motion required at start up	
Resolution (101001 Product Option)	10bits 1,024counts per rev 1265.6arc-secs 6144micro-rads	
Resolution (121001 Product Option)	12bits 4,096counts per rev 316.4arc-secs 1536micro-rads	
Resolution (141001 Product Option)	14bits 16,384counts per rev 79.1arc-secs 384micro-rads	
Resolution (161001 Product Option)	16bits 65,536counts per rev 19.77arc-secs 96micro-rads	
Resolution (171001 Product Option)	17bits 131,072counts per rev 2.47arc-secs 12micro-rads	
Repeatability	+/-1	count
Static Accuracy over 360°	≤353arc-seconds or ≤1.71milliradians	
Internal Position Update Period	<0.1	millisecond
Thermal Drift Coefficient	≤1.0	ppm/K Full-Scale
Max. Speed for Angle Measurement	10,000	r.p.m.
Max. Physical Speed	10,000	r.p.m.
Electrical		
Data Outputs	RS422 Compatible, supports SSI (Serial Synchronous Interface), asynchronous serial interface (ASI), SPI or BiSS-C.	
Power Supply	5VDC (4.5-8VDC) or 12VDC (4.5-14VDC)	VDC
Current Consumption	<100 (typically <75 and does not change significantly with voltage supply)	milliAmp
Reverse Polarity	PSU Reverse polarity protected to max. supply voltage	
Zero Setting	Zero Set or Reset to factory value via Electronics Module - Section 7.1	
Power Up Time To 1st Measurement	<75	millisecond
Environment		
Operating Temp.	Minus 45 to +85 (+65 at >8VDC power supply) Operation outside limits to be qualified by user. At temperatures >85Celsius, duration should be minimized. Options available below minus 60 Celsius operation: contact Celera Motion or local representative for details	
Storage Temp.	Minus 55 to +125	
Temperature Shock	MIL-STD-810G, Method 503.5, Procedure I-B (T1=-40 °C, T2=55 °C.)	
IP Rating - Rotor & Stator	IP67 for <60 minutes & 1m depth	
Humidity	RH 0-99% non-condensing - but unaffected by occasional condensation	
Salt Fog	Complies with DEF STAN 00-35 Pt 3 Iss. 4, Test CN2 Salt Mist Test	
Bio Hazards	Complies with DEF-STAN 00-35 Pt 4 Iss. 4 Section 11 (Hazards)	
Induced Dust & Sand	Complies with DEF STAN 00-35 Part 3 Issue 4, Test CL25 (Turbulent Dust) Cat 1	
Shock	IEC 60068-2-27 100g for 11ms - axial & radial - suitable for most airborne, marine & armoured vehicles MIL-STD-810G, Method 516.6, Procedure I-Functional Shock - axial and radial - 40 g 11 ms, sawtooth waveform	
Vibration	IEC 60068-2-6 20g for 10-2000Hz - axial and radial - suitable for most high vibration & airborne environments MIL-STD-810G, Method 514.6, Procedure I - axial and radial - Category 20, for tracked vehicles	
Environmental pressure range	0 to 4 (in other words vacuum to 4)	
Max. permissible press. change rate	1	
EMC Radiated Susceptibility	(Installed) Complies with IEC 61000-6-2 - suitable for fitment in harsh EMC environments	
EMC Radiated Emissions	(Installed) Complies with IEC 61000-6-4 - suitable for fitment adjacent to EMI sensitive devices	

Table 3 – Technical data

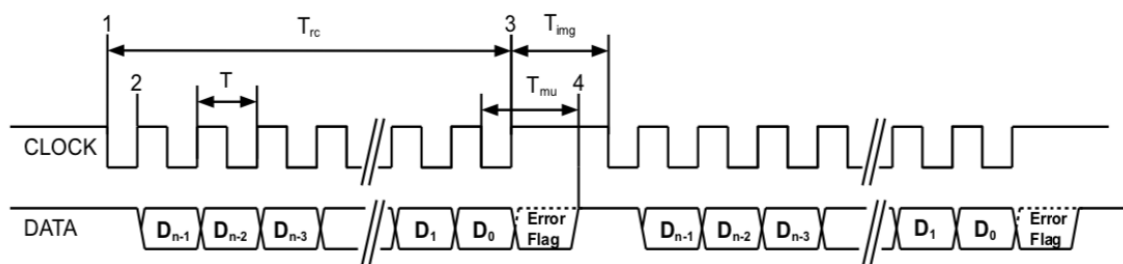
SSI (Synchronous Serial Interface) is a widely used serial interface between position sensors and controllers. It is used to transfer digital data from a peripheral device to a central unit (PLC or Host), through a minimum number of connections with respect to the resources necessary for transferring it in parallel, reducing the cost of wiring and the risk of errors.

This interface complies with the RS422 communication standard and implements a differential output for the DATA and a differential input for the CLOCK, which has a high immunity to both common and induced disturbances, as communication distances can be reached between peripherals and PLCs of considerable length.

The PLC sends a specific sequence of pulses to the clock line called the pulse or burst packet. This action causes the encoder to send the bits necessary for the formation of the data in synchronization with this pulse packet.

Most popular choice

SSI1 (n = 24)		
D23	PV	Position Valid Flag. Set to 1 when data is valid, otherwise 0 (the inverse of the ERROR FLAG).
D22	ZPD	Zero Point Default. Set to 1 when the Zero Point is at Factory Default, otherwise 0
D21-D0	PD[21:0]	Binary position data. If resolution of device is less than 22 bits, then the MSBs of this field are set to 0. The LSB of this field is in D0. When PV is 0, PD[21:0] value is not defined.



- T: Clock Period ($1/T = 100 \text{ kHz to } 2 \text{ MHz}$)
- T_{rc} : Read Cycle time: This is defined as $(n \times T) + (0.5 \times T)$
- T_{mu} : Message Update time. The time from last falling edge of clock to when new data is ready for transmission.
 $T_{mu} = 20\mu\text{s} \pm 1 \mu\text{s}$. The DATA line will be HIGH after this time indicating a new Read Cycle can be started.
- T_{img} : Intermessage Gap time. Must be $> T_{mu}$ otherwise position data will be indeterminate.
- n: The number of bits in the message (not including the Error Flag).
In idle state CLOCK and DATA are both HIGH

Fig.31 – Synchronous Serial Interface

Another possibility could be replacing the encoder with **inertial sensors**.

Inertial sensors are advanced technological devices able to measure some variables of the movement (called kinematic variables) of a body to which they are firmly attached. The body we are referring to can be an object or the human body or, more specifically, its body segment.

There are two main categories of inertial sensors: accelerometers and gyroscopes.

Accelerometer is an instrument for measuring acceleration or for detecting and measuring vibrations, there are different type of:

- *Piezoresistive bridge accelerometer*: this is a variant of the strain gauge bridge accelerometer, where piezoresistive sensors are used instead of strain gauges.

- *LVDT Accelerometer*: uses an LVDT (Linear Variable Differential Transformer) sensor. In these devices, the mass is composed of a ferromagnetic material and flows (suspended on springs or other elastic elements) inside a coil generating an induced current in the coils. A special circuit detects the position of the core with respect to the coils and generates an electrical signal proportional to the displacement.

- *Capacitive Accelerometer*: exploits the variation of the electrical capacity of a capacitor as the distance between its armatures varies. The ground (made of conductive material) is an armature, while the other is made on the fixed structure of the device. When the mass moves, the capacitance of the capacitor changes (which depends on the distance between the armatures) and a special circuit detects the change as a function of the position.

- *Piezoelectric Accelerometer*: uses the electrical signal generated by a piezoelectric crystal. The mass is suspended on the piezoelectric crystal, which, in this case, constitutes both the sensor and the elastic element. In the presence of an acceleration, the mass (which has a certain inertia) compresses the crystal.

- *Laser Accelerometer*: In this device a laser interferometer measures instant by instant the movement of the moving object, a computer connected to it makes the second derivative with respect to time, thus obtaining directly the acceleration value.

From accelerometers, as the word itself says, it is possible to derive a measure of the (linear) acceleration to which the body is subjected. From this, theoretically, one could obtain through a mathematical operation an estimate of speed (linear) and position. Unfortunately, these estimates are, at the present state of the art, so affected by errors that

they cannot be considered sufficiently reliable for the scientific world, but can be used, with appropriate caution, in some particular practical applications.

On the other hand, the gyroscope is a rotating physical device which, due to the law of conservation of the angular momentum, tends to maintain its axis of rotation oriented in a fixed direction. Essentially it consists of a toroid-shaped rotor that rotates around its axis, when the rotor is rotating its axis tends to remain parallel to itself and to oppose any attempt to change its orientation.

The main problem with gyroscopes is the presence of small offsets that cause signal drift and unacceptable errors during the integration process necessary to evaluate orientation changes.

For the current state of the art, these sensors can be integrated into the mechanical arm system for greater control over the initial position but are not able to replace an encoder completely due to low accuracy.

Design of pieces to block and change rotations

The second aim of the work is reviewing the design of pieces to block and change mobility of the mechanical arm.

The main feature must be the ease of removal of the pieces in order to change the rotation in action. To redesign new pieces, it was necessary to take sizes of the different parts of the system and use Solid Edge. The Laboratory Ampere has different type of 3D printers, so we decide to use them to test also different components.

Three-dimensional (3D) printing is one of the most versatile and revolutionary additive manufacturing (AM) techniques to create 3D objects with unique structure and many properties. Presently, various techniques such as fused deposition modeling (FDM), stereolithography apparatus (SLA), continuous liquid interface production (CLIP), digital light processing (DLP) and selective laser sintering (SLS) have been developed to form stereoscopic objects with complex architecture.

“In the late 1980s, S. Scott Crump developed FDM 3D printer and it was commercialized by Stratasys in 1990. With the 2009 expiration of the patent on this technology, people could use this type of printing without paying Stratasys for the right to do so, opening up commercial, DIY, and open-source (RepRap) 3D printer applications. Now, FDM has become the most widely used 3D printing method due to its simple-to-use, low-cost and environment-friendly features and is increasingly used in product development, prototyping and manufacturing processes in a variety of industries, including household appliances, automobile, toys, architecture, medical appliances, aircraft and aerospace” [32].

The following factors limit the application of FDM 3D printing: the mechanical strength of the FDM printed products are usually worse compared with injection modeling due to their weakness points between the layers, and also, the thermoplastic materials tend to shrink during the cooling process, resulting in warp of the printed products. However, for the pieces that we need, 3D printing is the best solution.

Fused deposition modeling uses material extrusion to print items, where a feedstock material is pushed through an extruder. In most fused filament fabrication 3D printing

machines, the feedstock material comes in the form of a filament wound onto a spool” [32].

FDM begins with a software process which processes an STL file (STereoLithography file format), mathematically slicing and orienting the model for the build process, created with Solid Edge.

The nozzle can be relocated in horizontal and vertical directions, and is assembled into a mechanical stage, that also can be moved in the **xy** plane. When the nozzle migrates over the table in an establish geometry, it deposits a thin bead of extruded plastic, called a “road” which solidifies quickly upon contact with substrate and/or roads deposited earlier. Repeating this action, solid layers are generated: the roads are deposited side by side within an enclosing domain boundary. Once a layer is completed, the platform is lowered in the **z direction** in order to start the next layer. This process continues until the printing of the object is completed.

During extrusion the thermoplastic filament is set up by mechanical pressure from rollers, into the liquefier, where it melts and is then extruded. Flow geometry of the extruder, heating method and the melt flow behavior of a non-Newtonian fluid are of main consideration in the part. The rollers are the only drive mechanism in the material distribution system: consequently, filament is under tensile stress upstream to the roller and under compression at the downstream side acting as a piston. Therefore, compressive stress is the driving force behind the extrusion process.

Usually, for FDM 3D printer are used thermoplastic materials like ABS, nylon, polylactic acid (PLA) and their blends. To enhance the mechanical properties of 3D printed thermoplastics, fiber-reinforced composites were used. However, addition of fibers often results in that the composites are susceptible to fracture during extrusion. Special additives may be necessary in the extrusion to help produce continuous and homogeneous filaments. In recent years, the emergence of nanocomposites has attracted great interest amongst researchers. By using small volume fractions of Nano additives, mechanical properties, heat distortion temperature and thermal stability of a polymer matrix can be improved.

In the Laboratory Primeca at INSA Lyon, it's possible to use UP mini plus: an original standard FDM 3D printing which has been employed for prototyping and final product creation in a wide array of industries.

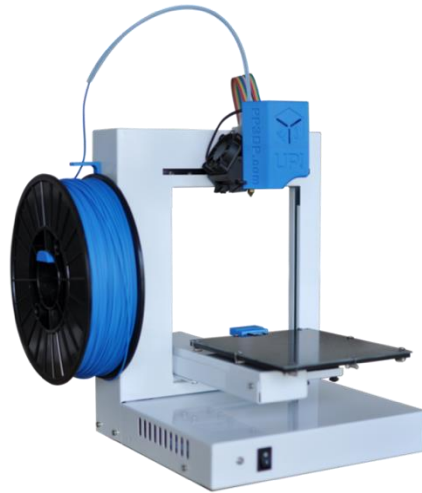


Fig.32 – UP Mini Plus

“A groundbreaking and time-saving feature, the UP Plus 2 was the first 3D printer in its class with an automatic platform calibration system. A probe’s sensor checks nine different points on the build surface for irregularities. If there is variation from one point to another, compensation settings are automatically entered into UP Studio. Print job removal and print surface cleaning are easy with the UP Plus 2. Simply snap the platform latches to secure and remove the print surface. Thanks to UP Studio’s custom nozzle and platform temperature control, the Plus 2 is capable of printing with a variety of filaments to match your purpose: ABS, PLA, PLA Composites, Polycarbonate, Bronze, Conductive, Nylon, Wood, ASA, PET, Flexible, Carbon Fiber and more” [30].

The best material, that respect our necessity, was the ABS, the right combination of the strength and hardness, gloss, toughness, and electrical insulation properties. “ABS is derived from acrylonitrile, butadiene, and styrene. Acrylonitrile is a synthetic monomer produced from propylene and ammonia; butadiene is a petroleum hydrocarbon obtained from the C4 fraction of steam cracking; styrene monomer is made by dehydrogenation of ethyl benzene a hydrocarbon obtained in the reaction of ethylene and benzene. A variety of modifications can be made to improve impact resistance, toughness, and heat resistance. The impact resistance can be amplified by increasing the proportions of polybutadiene in relation to styrene and also acrylonitrile,

although this causes changes in other properties. Impact resistance does not fall off rapidly at lower temperatures” [31]. Stability under load is excellent with limited loads. Therefore, by changing the proportions of its components, ABS can be prepared in different grades. There are two main categories of ABS: (1) for extrusion and (2) for injection moulding, i.e. high and medium impact strength. In general, ABS would have useful characteristics in a temperature range of -20 to 80 °C (-4 to 176 °F). ABS offers these advantages:

- Excellent impact, chemical and abrasion resistance
- Superior stiffness and strength
- Easily machined and thermoformed
- Easy to paint and glue
- Good dimensional stability
- Excellent electrical properties

Even though ABS plastics are used commonly for mechanical design projects, they also have electrical properties that are justly constant over an ample variety of frequencies. These properties are little affected by temperature and atmospheric humidity in the acceptable operating series of temperatures. ABS can be recycled, although it is not accepted by all recycling facilities.

“ABS is stable to decomposition under normal use and polymer processing conditions with exposure to carcinogens well below workplace exposure limits. However, at higher temperatures at or above 400 °C (750 °F) ABS can decompose into its constituents: butadiene (carcinogenic to humans), acrylonitrile (possibly carcinogenic to humans), and styrene. Ultrafine particles (UFPs) may be produced at lower temperatures during the 3D printing process. Concerns have been raised regarding airborne UFP concentrations generated while printing with ABS, as UFPs have been linked with adverse health effects” [31] . When it is used as a filament for the 3D printing process Fused Deposition Modeling it is suitable due to the high stability and various post-processing options (sanding, painting, gluing, filling), especially for the production of prototypes.

The primary needs of the prototype were to improve the quality of mechanical movements, including the design of new, simple components that could be made with the 3D printer.

After studying the mechanical structure and carrying out qualitative tests on the movement, it was decided to proceed with the construction of two types of components: the first, similar to a clip, to block the vertical bending movement; the second to give greater rigidity to the structure and block the degree of freedom of rotation on the horizontal plane.

I began the design by collecting dimensional data from the drawings and directly from the machine, so as to limit tolerance errors. I then drew several test components with the Solid Edge CAD system and, once I had analyzed and chosen the most suitable ones, I converted them into .stl format, which stands for Stereo Lithography format. The .stl file is represented by meshes, which are basically triangular surfaces. If the model has a large number of meshes, the approximation, and therefore the quality, with which it is reproduced will be better. This characteristic is what is known in the modelling field as 'resolution'. Most modelling software allows you to decide the level of resolution of the STL file.

Following the .stl file of the pieces specially drawn on Solid Edge.

The first ones are the two clips, elastic and at the same time rigid, given their shape, to block the vertical rotation of the mechanical arm.

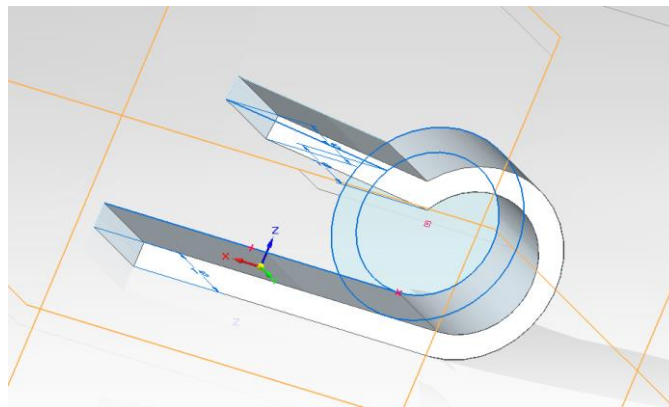


Fig.33 – Clip's drawing

The second ones are two components, which together form a rigid piece capable of blocking the horizontal rotation of the structure.

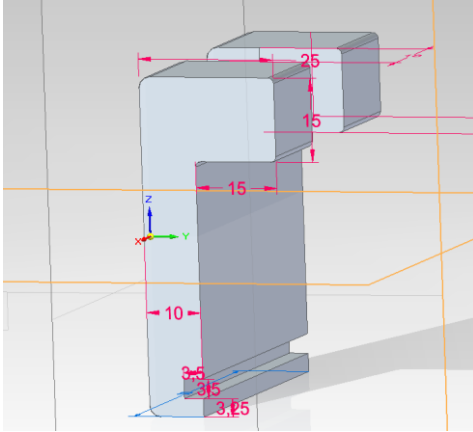


Fig.34 – Component 1

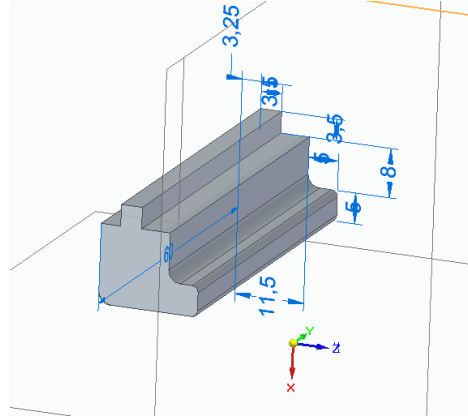


Fig.35 – Component 2

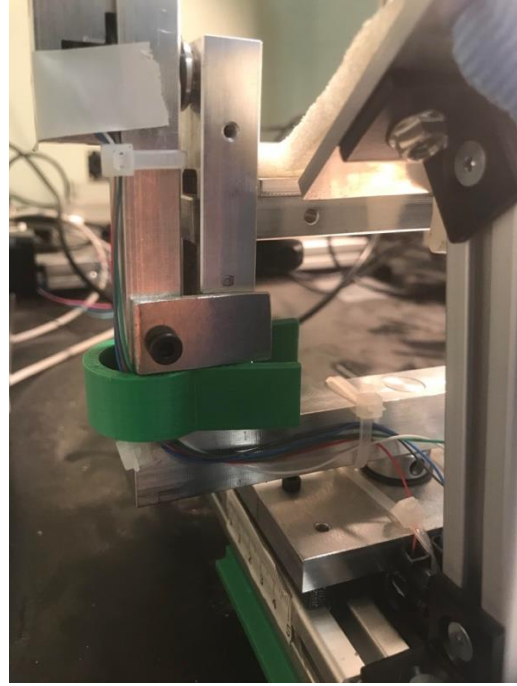
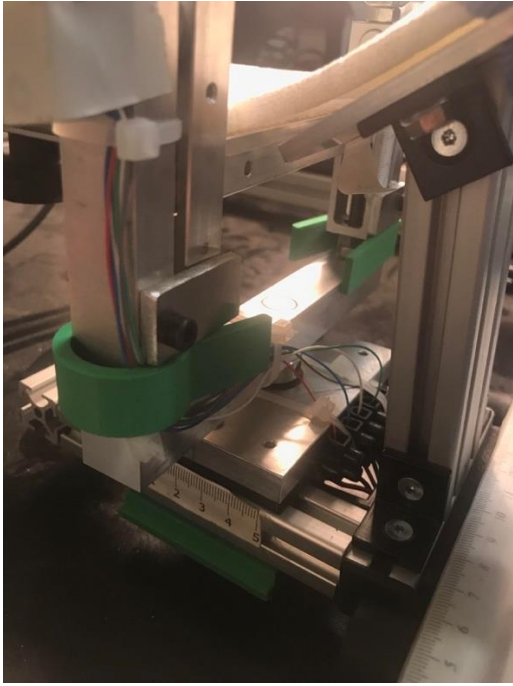


Fig.36/37 – Clips on the prototype

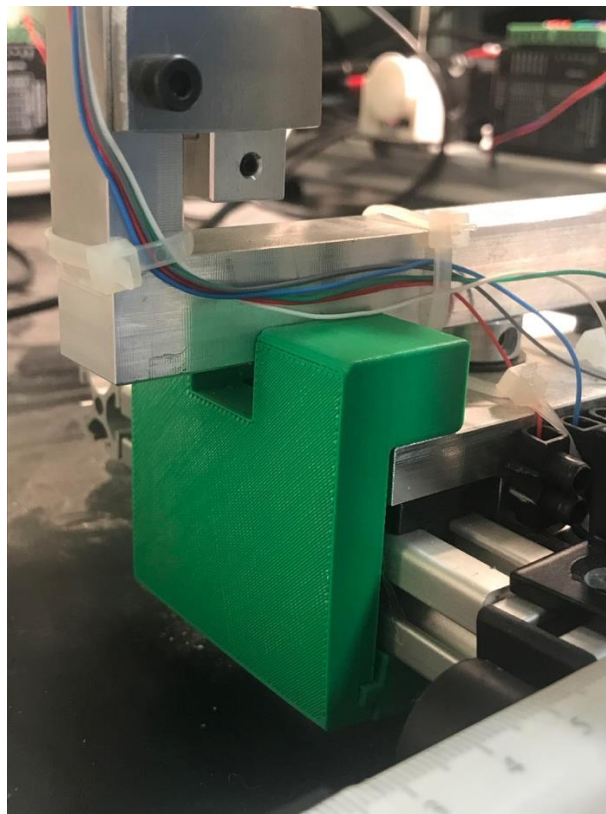


Fig.38 – Piece to block horizontal rotation

Control

The aim of this part of the project is to create a computer program, which allow to control better and know in real time the position of mechanical arms, to add to the sensors system. The first idea was to make a Matlab program, in accordance with the control system already in place for dSpace communication, but at the end the choice was to work with an OpenMV Camera, introducing a specific device for image detection and analysis.

“The OpenMV H7 Camera is a small, low power, microcontroller board which allows you to easily implement applications using machine vision in the real-world. It’s possible to program the OpenMV Cam in high level Python scripts instead of C/C++. This makes it easier to deal with the complex outputs of machine vision algorithms and working with high level data structures.

The OpenMV H7 comes with a OV7725 image sensor is capable of taking 640x480 8-bit Grayscale images or 640x480 16-bit RGB565 images at 60 FPS when the resolution is above 320x240 and 120 FPS when it is below. Additionally, the OpenMV H7 now features removable camera modules which allow you to use the module with Global Shutter and FLIR Lepton sensors for serious computer vision applications.

The STM32H743VI ARM Cortex M7 processor running at 400 MHz with 1MB of RAM and 2 MB of flash. All I/O pins output 3.3V and are 5V tolerant. The processor has the following I/O interfaces:

- Full speed USB (12Mbs) interface to your computer. Your OpenMV Cam will appear as a Virtual COM Port and a USB Flash Drive when plugged in.
- μ SD Card socket capable of 100Mbs reads/writes which allows your OpenMV Cam to record video and easy pull machine vision assets off of the μ SD card.
- SPI bus that can run up to 100Mbs allowing you to easily stream image data off the system to either the LCD Shield, the WiFi Shield, or another microcontroller.
- I2C Bus, CAN Bus, and an Asynchronous Serial Bus (TX/RX) for interfacing with other microcontrollers and sensors.
- 12-bit ADC and a 12-bit DAC.

- Three I/O pins for servo control.
- Interrupts and PWM on all I/O pins (there are 10 I/O pins on the board).
- RGB LED and two high power 850nm IR LEDs.” [34]

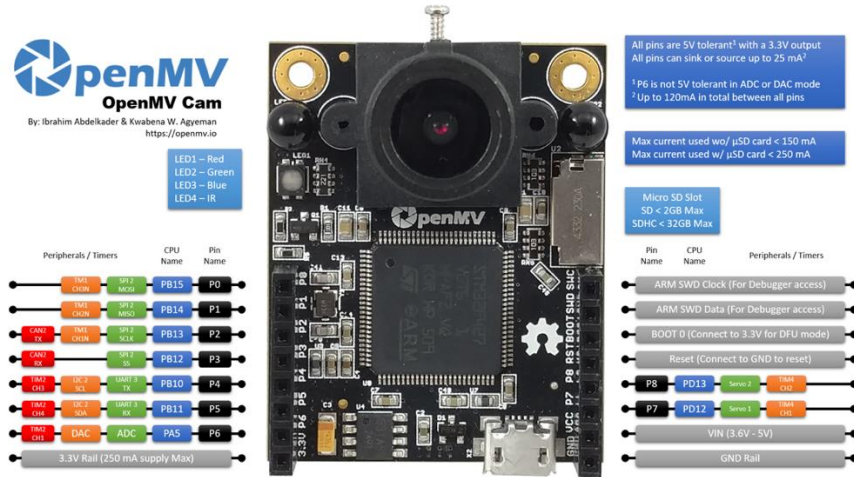


Fig.39 – OpenMV Cam

The idea of the computer program is to detect a color, draw a box around the area and track in real time the position of the center. Given the environmental conditions for testing and using the prototype, which are still being defined, it was decided to use yellow, a colour that is more easily identifiable in a wide range of colour scales and atmospheric light quantities. For this reason, a yellow sticker had to be placed at the base of the mechanical arm handle.

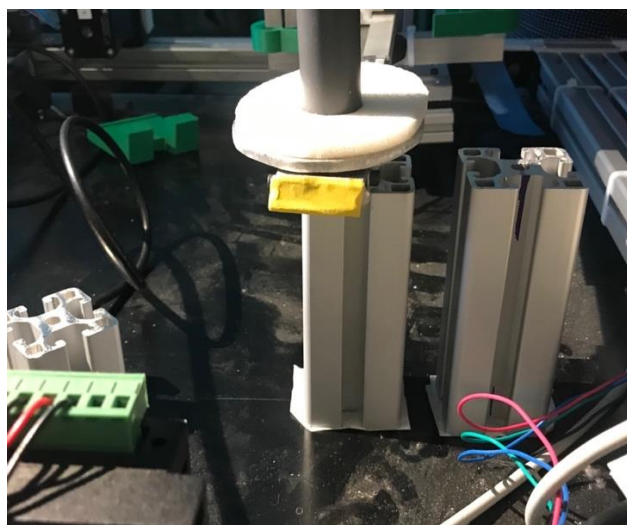


Fig.40 – Yellow sticker to detect

Follow the written program:

```
# Single Color Code Tracking

import sensor, image, time, math

thresholds_index = 0 #for yellow

# Color Tracking Thresholds (L Min, L Max, A Min, A Max, B Min, B Max)

# The below thresholds track in general yellow things.

thresholds = [(50,100,-20,20,30,100)] #generic_yellow_thresholds

sensor.reset()

sensor.set_pixformat(sensor.RGB565)

sensor.set_framesize(sensor.QVGA) #320x240

sensor.skip_frames(30)

sensor.set_auto_gain(False) # must be turned off for color tracking

sensor.set_auto_whitebal(False) # must be turned off for color tracking

clock = time.clock()

# Only blobs that with more pixels than "pixel_threshold" and more area than
"area_threshold" are returned by "find_blobs" below. Change "pixels_threshold"
and "area_threshold" if you change the camera resolution. "merge=True" must
be set to merge overlapping color blobs for color codes.

while(True):

    clock.tick()
```

```

clock.avg()

img = sensor.snapshot()

for blob in img.find_blobs([thresholds[thresholds_index]],
pixels_threshold=200, area_threshold=200, merge=True):

    # These values are stable all the time.

    img.draw_rectangle(blob.rect())

    img.draw_cross(blob.cx(), blob.cy())

    print("x:", blob.cx(), end=")

    print(" y:", blob.cy())

    print(clock.avg())

```

In OpenMV Cam program, the basis of the colour identification system is CIELAB technique.

Colors might be noticed in different ways depending on individuals and may be showed differently depending on the peripheral display tools.

“The International Lighting Commission (*Commission Internationale de l'Eclairage*, CIE) thus defined standards allowing a color to be defined, independently from the peripheral devices used. For this purpose, the *CIE* defined criteria based on the perception of color by the human eye, thanks to a triple stimulus.

In 1931, the CIE worked out the *xyY* colorimetric system which allows colors to be represented according to their chromaticity (X and Y axes) and their luminance (Y-axis). The *chromaticity diagram* (or *chromatic diagram*), resulting from a mathematical transformation, represents pure colors on the periphery, i.e. the monochromatic radiation corresponding to the colors of the spectrum (the colors of the rainbow), indicated by their

wavelength” [28]. The line connecting the ends of the diagram (thus connecting the two ends of the visible spectrum) is known as the *line of purples*, because it corresponds to the color purple, made up of the two monochromatic rays blue (420 nm) and red (680 nm):

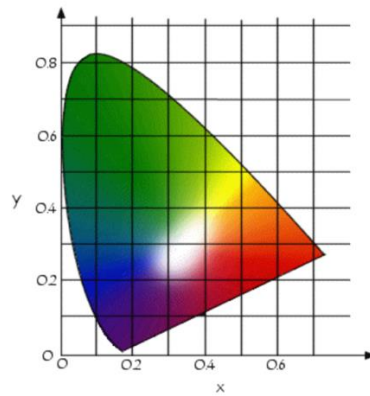


Fig.41 – CIE system

The *gamut* of a display device is generally represented by tracing, in the chromatic diagram, a polygon containing all the colors which it is capable of producing.

However, this purely mathematical type of representation does not take into consideration physiological factors, i.e. color perception by the human eye, which results in a chromaticity diagram that leaves too much space for greens.

Finally, in 1976, in order to overcome the problems with the xyY , model, the CIE developed the $\mathbf{L}^*\mathbf{a}^*\mathbf{b}^*$ colorimetric model (also known as the *CIE Lab*), in which a color is indicated by three values:

- **L**, lightness, expressed as a percentage (0 for black to 100 for white)
- **a** and **b** two color ranges, from green to red and from blue to yellow respectively, with values ranging from -120 to +120.

The *Lab* mode thus covers the entire spectrum visible to the human eye and represents it in a uniform way. It is typically used when graphics for print have to be converted from RGB to CMYK, as the CIELAB gamut includes both the gamuts of the RGB and CMYK color models. Because three parameters are monitored, the space itself is a three-dimensional real number space, which enables infinity possible colors. In practice, the space is generally mapped into a three-dimensional integer space for digital

representation, and thus the L^* , a^* , and b^* values are usually absolute, with a pre-defined range.

It is a mode that is very much used in industry, but not much favored by most software since it is difficult to handle. The CIE models are not intuitive, however the use of these guarantees that a color created according to these models will be seen in the same way by everyone and it aspires to perceptual uniformity.

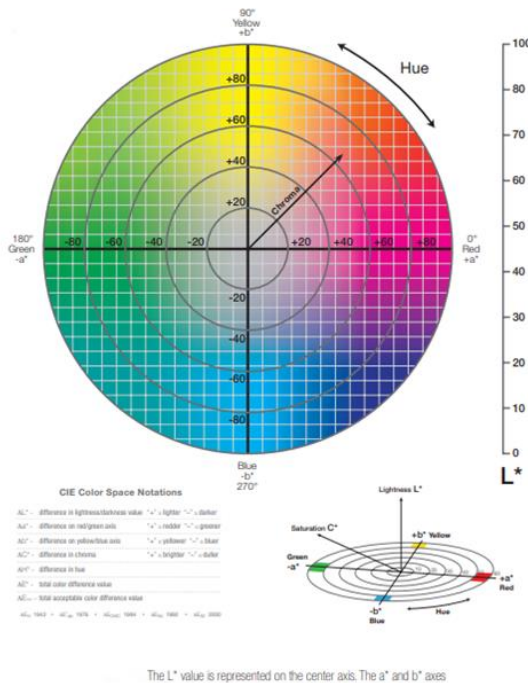


Fig.42 – CIELAB model

The interface, that allow to create a connection tool between the robotics of the device and the computer that contains the "Simulink" model, has been created with ControlDesk instrumentation and dSPACE testing software. This software allows to quickly develop an interface connected to a dSPACE board, which is convenient for our prototype.

This type of dSPACE board is nothing more than a PACE board (Equivalent to Arduino) and it is more suitable for prototyping: the connections are made via BNC cables, so they are easily scalable, and the interface is directly associated with ControlDesk without any code to write. The last advantage is its direct connection with MATLAB. A Simulink model can be loaded into a ControlDesk "experiment", its variables are then directly adjustable and the output values of the board (i.e. at the device input) can be viewed.

The prototype consists of 6 motors connected to reels that allow to move one of the subject's limbs. The latter puts his limb down and holds a handle in his hand. From this handle cables connect to the motor reels. Each motor can be controlled independently. The program associated with the prototype allows to follow predefined trajectories in 2 planes (sagittal plane and horizontal plane) according to 2 modalities (ipsilateral and contralateral).

Thus in the horizontal plane, the operator can choose that the subject moves from -20° , -10° , 10° or 20° . Negative angles refer to the abduction movement (the forearm moves away from the body's centre line). Positive angles concerning the adduction movement (the forearm approaches the body's centre line).

In the sagittal plane, the operator can choose that the subject moves 20° ou 40° .

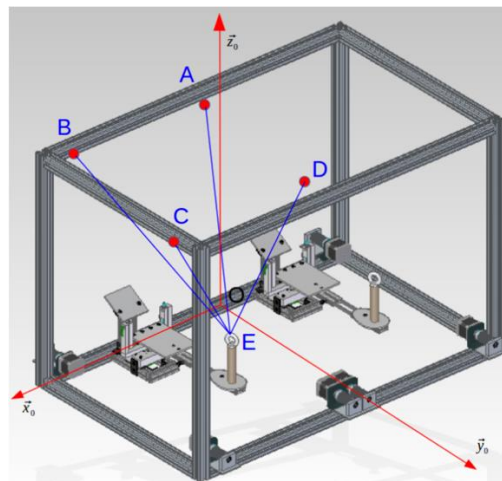


Fig.43 – Prototype structure

On each motor, a reel is mounted. By turning it in one direction, it rolls up a cable that allows the handle and therefore the subject's limb to be moved. By turning in the other direction, the cable unwinds and by the action of gravity the mechanical arm moves in another direction. Figure 43 shows a schematic diagram of the cables' prototype. In this diagram, only the right arm marking is shown for the sake of clarity in the diagram. For the same reason, the cables shown in blue in the diagram are not fully represented, so the constant length part connecting the pulley to the reel is not present.

It should be noted that:

- point O is the origin (intersection of the vectors \vec{x}_0 , \vec{y}_0 and \vec{z}_0) of the marker linked to the right arm. For the left arm the origin is not the same, but the vectors remain in the same direction.

- points A, B, C and D correspond to the position of the pulleys.

- Point E is the intersection of all cables and corresponds to the center of the ring mounted on the

handle that the subject holds.

- the cables are named as follows:

- The cable connecting A, E and B is connected to motor 1 and is called L₁.

- The cable connecting C and E is connected to motor 2 and is called L₂.

- The cable connecting D and E is connected to motor 3 and is called L₃.

For the left arm, the same rule is applied and the lengths are called L₄, L₅ and L₆.

To adapt the prototype to the size of the subject, there are 4 parameters:

- *the width of the shoulders called position x of the elbow*: this adjustment is done simply by unscrewing one of the two plastic cylinders, called the pad, which blocks the movable part along the \vec{x}_0 axis. Once this block has been removed, it is possible to move the movable arm support horizontally. Remember to replace the stud and move the stud on the other side to block the movable support.

The value of this setting can be read directly from the scale. There is a mark on the vertical part that indicates the middle of the movable support. This value must be entered in the software in the x elbow position box.

- *the position of the elbow called the y-position of the elbow*: this adjustment is made by unscrewing (or screwing) the lever on the left photo in To avoid having to lift the prototype, it is possible to pull the joystick outwards. This disengages the lever to return to the initial position of the lever and unscrews (or screws) it. Once the bracket is correctly positioned, simply screw the lever back on to lock the bracket.

The value of this setting can be read on the other side on the scale. There is a mark on the vertical part that indicates the middle of the movable support. This value must be entered in the software in the elbow position box.

- *the height of the elbow called the z position of the elbow*: this adjustment is done simply by unscrewing (or screwing) the wing nut located in need of the screw as shown in the picture opposite.

The value of this setting can be read directly from the scale. Since the foam is deformed, the value to be read is located on the aluminum plate under the foam as shown in the picture below. This value - true to be entered in the software in the box z elbow position.

- *the length of the forearm called position L arm*: this adjustment is done from below. Simply unscrew the knob nut, choose the desired length and screw it back in to lock the position.

The value of this setting can be read directly from the scale. The value is read from the extremity of the aluminum tray which translates as shown in the picture opposite. This value must be entered in the software in the box L arm position.

These parameters are shown in following figure, in this diagram it is the right arm, but the same system and nomenclature exists for the left arm.

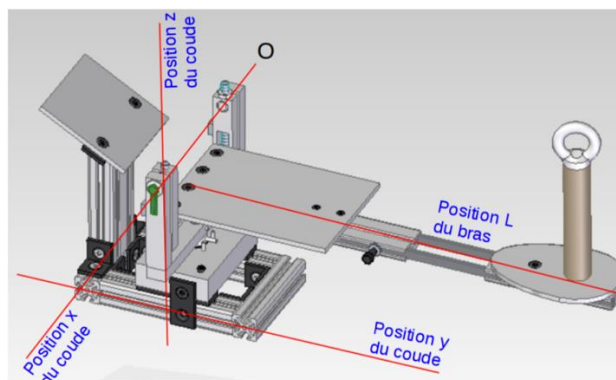


Fig.43 – Axis on the mechanical arms

Boxes on display

Below (Fig. 44) there are the functions of the boxes on the display of ControlDesk program control.

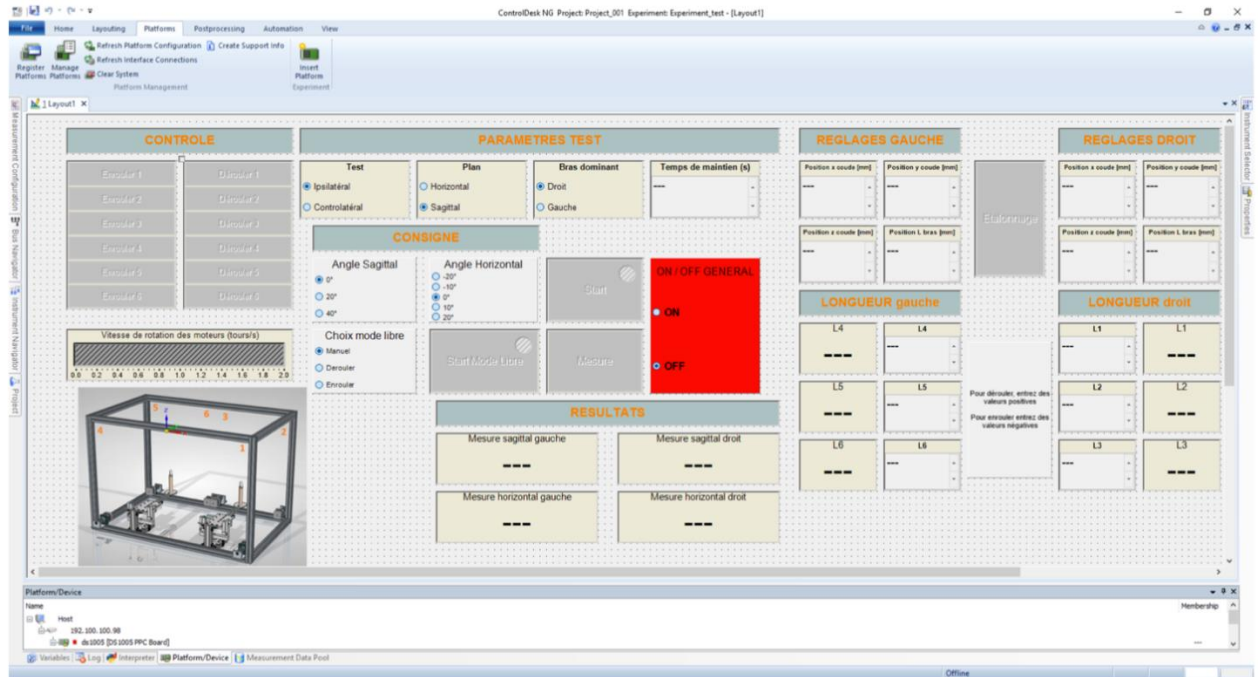


Fig.44 – ControlDesk

1. Online / offline

This allows you to activate/deactivate the online control via the interface. So as long as the interface is Offline, pressing a button has no effect. To check the prototype, you must first click on Go Online. Once the software is online, it is possible to control the prototype in real time.

The Start Measuring icon will not be used because the measurement will be automatically activated when the measurement is taken. However, it may be necessary to use the Stop Measuring button.

2. Initialization of geometric parameters

This allows the geometric parameters of the prototype to be updated. Indeed, the prototype must be adjusted to adapt to the size of the subject. For these settings is necessary to indicate the 4 measurements made during the prototype settings and click on

the Calibration button to validate them. If this step is not performed, the results and behaviour of the prototype may be totally false and/or unpredictable.

3. Information on cable lengths

This allows you to know the length of the cable between the center of the handle ring that the subject holds in his hand and the pulley corresponding to the cable concerned. It is also possible to wind or unwind one of the 6 cables according to the desired length. A priori this area is mainly for information purposes and will not be used during the use of the prototype.

4. Initialization of the experiment parameters

This allows you to define the type of experiment to be performed (ipsilateral or contralateral), the execution plane of the movement (horizontal or sagittal), the arm concerned (left or right) and the time to hold the arm at the desired angle in the case of an ipsilateral experiment (by default this value is equal to 3 seconds).

5. Definition of instructions This allows you to:

- Define the desired angle according to the studied movement (20° ou 40° pour a movement in the sagittal plane and -20°, -10°, 10° or 20° dans the horizontal plane).
- Activate the movement of the prototype after pressing the Start button
- Make a measurement after pressing the Measurement button
- Define (automatically or manually) the length of the cables to be wound or unwound by clicking on the Start Free Mode button.

6. Real-time measurement display

As the name implies, this area allows you to know the angular value of the sensors and therefore the amplitude of the subject's movement.

7. Manual control

This allows each motor to be controlled independently. This may be necessary to prepare the prototype, tighten or loosen the cables, reset the prototype. The drawing below shows the position of each pulley (and therefore each motor) and their number.

It is also possible to change the motor speed value during these operations via the sliding bar below. However, this operation will rarely be necessary. The default value (1 rpm) is generally sufficient.

8. Emergency stop

In addition to the mushroom button to stop the engines, there is another emergency stop. This one is present in the red box where you just have to click on Off in case of problem. Before reactivating the prototype, check that the subject is ready, that there is no green light on the interface (at the Start and Start Free Mode buttons) and that the initial conditions are good (both angles must be at 0°).

Execution of tests

To perform a movement on the prototype, simply click on the Start button. A green icon appears on this button to indicate that a movement is in progress, you must not touch anything while the icon is on (except the emergency stop button of course). The selected arm will move until it reaches the desired value in the desired plane. In the case of an ipsilateral test, it will remain in position for N seconds where N is the value indicated in the test parameters before returning to its initial position. In the case of a contralateral test, it will return to its initial position when the operator has clicked on the Measurement button.

At the first vertical tests in ipsilateral mode, I repeat the execution a lot of times changing the position of camera in front of the prototype. In this way was possible detecting that the distance of camera is a fundamental parameter for the success of points vision, because if the camera is too near to the mechanical arm it identifies a distorted image and the box center isn't recognized on the same y axis (same y pixel).

Best data were noted at 30 cm of distance from sticker, at a height of 14 cm in relation to the plane, in order to have an optimised viewing of the test workstation.

It's possible to convert number of pixels in distance in cm with the following formula:

$$d [cm] = \left(\frac{\text{number of pixels [pixel]}}{\text{resolution DPI} \left[\frac{\text{pixel}}{\text{inches}} \right]} \right) \cdot 2.54 \left[\frac{\text{cm}}{\text{inches}} \right]$$

Z pixel	X pixel	Z [cm]
169	133	23,6
168	134	23,5
161	134	22,5
155	134	21,7
148	134	20,7
142	134	19,8
136	134	19,0
130	134	18,2
124	134	17,3

118	134	16,5
112	134	15,6
106	133	14,8
102	133	14,3
107	134	14,9
112	134	15,6
117	134	16,3
122	134	17,0
127	134	17,7
133	134	18,6
138	134	19,3
143	134	20,0
149	134	20,8
155	133	21,7
160	133	22,4
167	133	23,3
167	134	23,3
168	134	23,5

The program also prints the time gap between two point detected, with these is possible plot the trajectory of the yellow rectangular sticker.

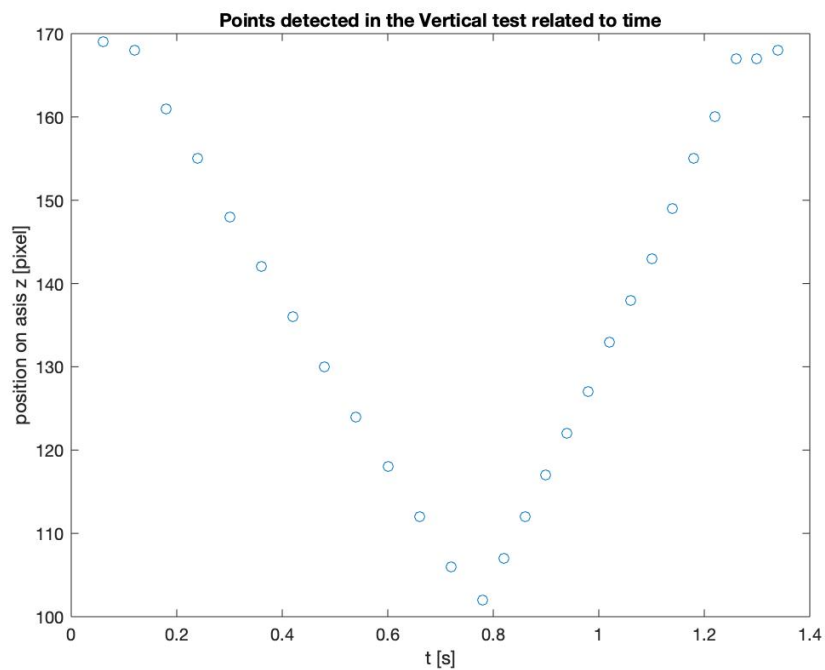
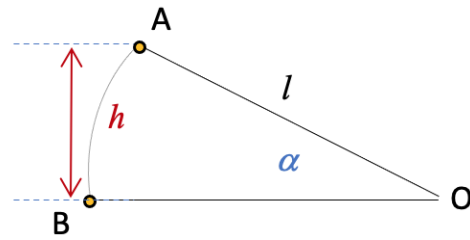


Fig.45 – Trajectory detected

Finally, to verify that the data captured by the camera can actually be useful to improve the control on the prototype, a geometric check is performed according to the following scheme:



$$h = l \sin \alpha \quad \alpha = \arcsin\left(\frac{h}{l}\right)$$

The vertical range length between the maximum height (point A) and the starter point of rotation (point B), around the center of rotation (point O), is then calculated, thus defining the value h. While as value l, is assumed the length of the moving mechanical arm, in this case 30 cm.

These gives an alpha value equal to 18° , not corresponding to the real value imposed by the dSpace computer program.

This difference is probably due to the type of lens the camera is equipped with (lens 2.8 mm), which is a fisheye camera: an ultra-wide-angle lens that produces strong visual distortion intended to create a wide panoramic or hemispherical image.

FOCAL LENGTH

& angle of view guide

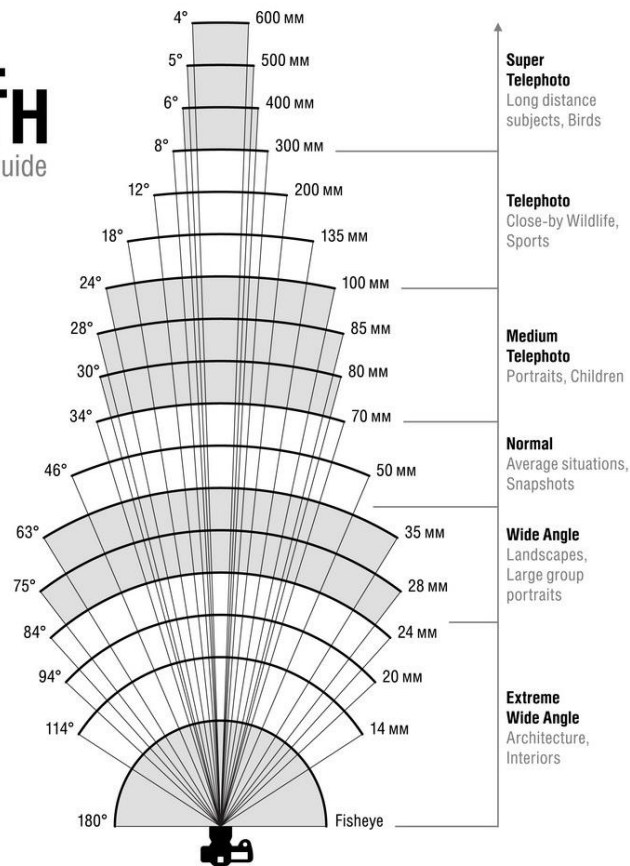


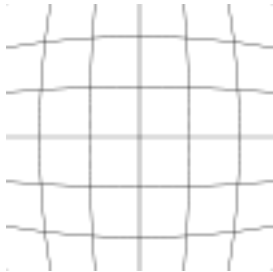
Fig.46 – Different type of cameras

Fisheye lenses achieve extremely wide angles of view. Instead of producing images with straight lines of perspective (rectilinear images), fisheye lenses use a special mapping, which gives images a characteristic convex non-rectilinear appearance.

Optical distortion occurs when the points in the object plane that make up a certain figure correspond to images that do not make up a similar figure. This phenomenon is largely due to the fact that the outer surfaces of the lenses are curved or spherical. In order to correct the distortion, symmetrical optical systems are used so that distortions of the opposite sign are introduced into them, which cancel out the distortion present in the image.

In geometric optics, **distortion** is defined as a deviation from rectilinear projection. It is considered as a form of optical anomaly.

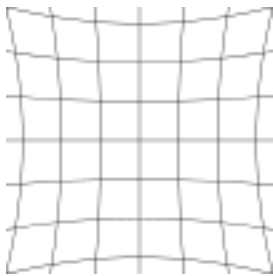
Even if distortion can be irregular or follow many patterns, the most common ones are radially symmetric developing from the symmetry of a photographic lens. These *radial distortions* can usually be classified as either *barrel* distortions or *pincushion* distortions.



Barrel distortion

In barrel distortion, image magnification decreases with distance from the optical axis. The apparent effect is that of an image which has been mapped around a sphere (or barrel). Fisheye lenses, which take hemispherical views, utilize this type of distortion as a way to map an infinitely wide object plane into a finite image area. In a zoom lens barrel distortion appears in the middle of the lens's focal length range and is worst at the wide-angle end of the range.

Fig.47– Barrel vision



Pincushion distortion

In pincushion distortion, image magnification increases with the distance from the optical axis. The visible effect is that lines that do not go through the centre of the image are bowed inwards, towards the centre of the image, like a pincushion.

Fig.48– Pincushion vision

Mathematically, barrel and pincushion distortion are quadratic, meaning they increase as the *square* of distance from the center. In mustache distortion the quartic (degree 4) term is significant: in the center, the degree 2-barrel distortion is dominant, while at the edge the degree 4 distortion in the pincushion direction dominates. Other distortions are in principle possible – pincushion in center and barrel at the edge, or higher order distortions (degree 6, degree 8) – but do not generally occur in practical lenses, and higher order distortions are small relative to the main barrel and pincushion effects.

A possible solution is to further increase the recording distance to require the movement in the top focus area of the sensor.

Sensor Array Center

Figure 13 OV7725 Sensor Array Center

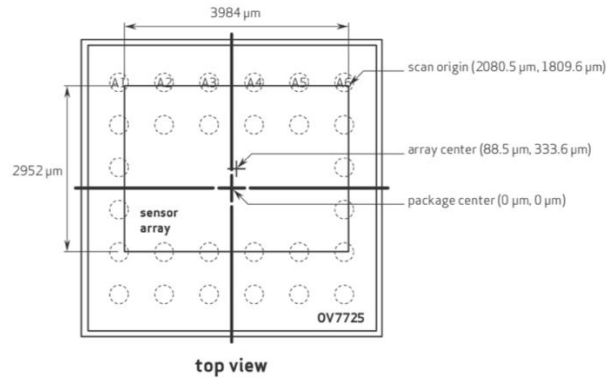


Fig.49– Sensor Array Center

Despite this, in general it's possible to find a way to correct the barrel distortion, adding specific lines in the MicroPython program on OpenMV:

```
img = sensor.snapshot().lens_corr(strength=1.8, zoom=1.0)
```

In this way the effect of the lens, since it's wide angle to see more, it's correct. The initial idea of OpenMV is to have the lens about 110 degree field of view, more than standard webcams of about 90, but for our aim it is not useful.

It's necessary also to add this:

```
sensor.set_framesize (sensor.HQVGA) #240x160
```

to reduce the resolution, because at the moment the system doesn't have enough RAM to work with a 320x240 resolution with VGA images and lens correction requires to allocate a temporary image.

After doing again tests, the result is different from the value that we aspect about 0.55°: that is the accuracy of this model.

This should be improved with the new encoder and also probably with a major space to work, putting the camera also far from 37 cm of the yellow sticker (the best distance found during tests).

Geometrical tests

A series tests were carried out with the prototype of which I knew exactly the distance in centimeters and, through the detection of pixel points and geometric transformation, verified that the two dimensions coincided.

Specifically, I used a fixed metal rod as a support to identify the detected starting point. Then I chose a series of other bars at different heights, which I noted down: this is the first value useful for comparison.

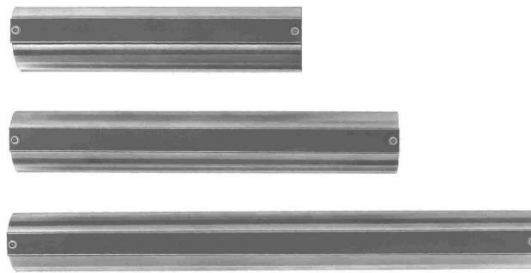


Fig. 50 – Metal rods

During the test, I initially placed the mechanical arm on the fixed bar, noting the starting pixel value detected by the program. Afterwards I placed on the starting bar the others of which I knew the measure and I placed on this structure composed by the arm of the prototype. The distance between the camera and the yellow point is always the same ($L=37$ cm).

Following the comparisons of values, collected during geometrical tests:

	<i>[pixel]</i>	<i>[cm]</i>
Start pix	112	21,72
Final pix	101	19,58
Measured value		2,13
Expected value		2,1
Gap		0,03

	<i>[pixel]</i>	<i>[cm]</i>
Start pix	113	21,91
Final pix	88	17,06
Measured value		4,85
Expected value		4,5
Gap		0,35

	<i>[pixel]</i>	<i>[cm]</i>
Start pix	112	21,72
Final pix	69	13,38
Measured value		8,34
Expected value		7,5
Gap		1,03

	<i>[pixel]</i>	<i>[cm]</i>
Start pix	112	21,72
Final pix	63	12,22
Measured value		9,5
Expected value		9
Gap		0,5

	<i>[pixel]</i>	<i>[cm]</i>
Start pix	112	21,72
Final pix	54	10,47
Measured value		11,25
Expected value		10
Gap		1,25

Note how the gap is increasing as the height of the bar positioned on the fixed one increases. A possible explanation is that as the mechanical arm becomes more and more at an angle to the camera, as the yellow point tilts and is detected with a different shape from the camera. As a result, the program prints the coordinates of a box in real time, which is actually subject to visual distortion.

For this reason, I repeat a same test but in the horizontal plane. In this case I used two bars of the same height and modified the horizontal distance between them. For greater precision, I added lines as indicators of the starting and the end point and then verified that the distance measured was equal to that obtained from the camera vision.

Following the comparisons of values:

	<i>[pixel]</i>	<i>[cm]</i>
Start pix	67	12,99
Final pix	124	24,04
Measured value		11,05
Expected value		11
Gap		0,05

	<i>[pixel]</i>	<i>[cm]</i>
Start pix	79	15,32
Final pix	105	20,36
Measured value		5,04
Expected value		5
Gap		0,04

	<i>[pixel]</i>	<i>[cm]</i>
Start pix	67	12,99
Final pix	112	21,72
Measured value		8,73
Expected value		8,6
Gap		0,13

	<i>[pixel]</i>	<i>[cm]</i>
Start pix	61	11,83
Final pix	133	25,79
Measured value		13,96
Expected value		13,8
Gap		0,16

See how the gaps have a very small value and therefore how the optical distortion is not actually present in the case of horizontal movement, because the camera does not recognize changes in the shape of the box around the yellow point.

The method is therefore applicable for ipsilateral tests and to be improved for sagittal ones.

Possible solutions could be a greater distance from the chamber with a more accentuated light, in order to improve recognition.

Arduino

In order to try to continuously improve the prototype, it is necessary to create a closed control system, so that the data stream produced by the camera can be processed in a microprocessor that can analyse them. Arduino, which is widely used in prototype development as a microcontroller programmable with the C language, therefore emerged as a suitable device to try and implement a replacement for the dSpace board.

Arduino is an open-source board, i.e. with a free license, used to build robotics, electronics and automation projects. It is a microcontroller programmable board including a software part, or IDE, which runs on a computer and is used to write and load computer code (in "C" language) into the board itself.

The Arduino project was created to allow creative artists, designers and planners to prototype and design their ideas without much technical knowledge. At its base there is the idea of making the creation of electronic projects faster and easier but above all easy and affordable for everyone.

The peculiarity of this product lies mainly in its modularity, expandability and versatility, allowing all fans of electronics, robotics or even software/firmware to interface with any object of this type.

There are different versions of this board, which differ in terms of calculation capacity, size, mode of communication with outdoor environments, etc.. In this article we will focus on the Arduino Mega 2560 version.

This model, compared to the previous ones, is characterized by a greater number of input/output ports and a greater memory for sketches (set-up + loop), that is the lists of commands that the board will have to process.

This article will show in detail the hardware features of the board and will also provide some hints of the software used to program the board and load the code.

How it is made

The Arduino Mega 2560 consists of an ATmega2560 microcontroller, 54 digital and 16 analog pins, 4 UART serial ports, a 16 MHz crystal oscillator, a USB port and power jack, an ICSP header and a reset button.

It has three types of memory: Flash, SRAM and EPROM. The card works at a nominal voltage of 5V and supports a maximum current of 40 mA.

As for the physical dimensions, Arduino Mega, compared to its predecessor, is more extended especially in length, measuring 101.52 mm, while the width is almost unchanged (53.3 mm). The weight is 37g.

In order to use the board, simply connect it to a PC via a USB cable or power it via an external source. Arduino Mega is compatible with most of the expansion boards, the so-called shields designed for the other versions of Arduino (UNO, Duemilanove, Diecimila). In the same way, it is possible to load and run most of the codes developed for the other versions, without having to make changes or have compatibility problems.

Microcontroller

The following figure shows the "brain" of Arduino Mega.



Program Memory Type	Flash
Program Memory (KB)	256
CPU Speed (MIPS)	16
RAM Bytes	8,192
Data EPROM (Bytes)	4096
Digital Communication Peripherals	4-UART, 5-SPI, 1-I2C
Capture/Compare/PWM Peripherals	4 Input Capture, 4 CCP, 16PWM
Timers	2 x 8-bit, 4 x 16-bit
Comparators	1
Temperature Range (C)	-40 to 85
Operating Voltage Range (V)	1.8 to 5.5
Pin Count	100

Fig.51– Microcontroller Arduino Mega

It is an 8-bit microcontroller of AVR-RISC type that integrates a 256 KB flash memory for code storage, an 8 KB SRAM and a 4KB EPROM (that can be read through the EPROM library), an oscillator, I/O ports and add-ons such as ADC, DAC, counters and timers. The device is able to reach a throughput of 16 MIPS at 16 MHz operating at a nominal voltage of 5V.

ATMega needs a clock with a frequency of 16 MHz to operate; for this reason a high frequency oscillating circuit is required. For this reason, we find integrated in the board an oscillator, based on oscillations of a piezoelectric material (quartz).

Power supply

The Arduino Mega can be powered in 2 ways: through the USB port or through an external source (AC-DC adapter or battery) using a power jack. In this case you have to use a 2.1 mm connector with the positive in the middle.

Next to the Power Jack there is a voltage regulator, whose task is to make stable (i.e. without excessive peaks) the voltage supplied to the components.

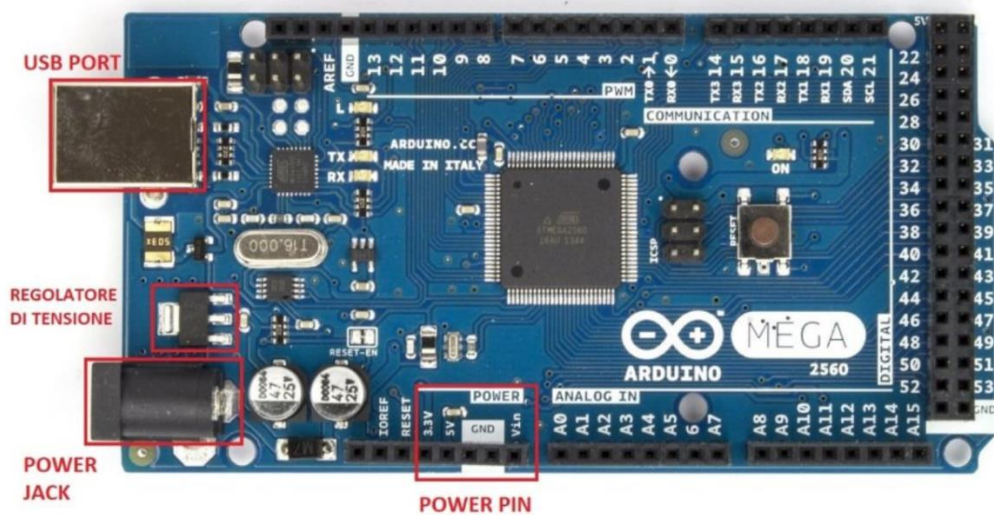


Fig.52 – Arduino Mega

The operating voltage of the card is between 6 and 22 volts, however, if you supply the card with a voltage lower than 7V or higher than 12V there could be malfunctions or instability. In fact providing a voltage lower than 7V consequently the 5V pins may not reach the nominal voltage value making the card unstable. In the second case, supplying the Arduino with a voltage higher than 12V, the voltage regulator could overheat with consequent damage to the board.

The advice is therefore to stay in the 7-12 volts range.

As for the output voltage, you can choose between two different values: 5V and 3.3V. Four power supply pins are available:

VIN pin, it corresponds to the input voltage of the card when you decide to supply it through an external source. More in detail, you can use this voltage in case the input arrives through the power jack.

Pin 5V, is used to power the microcontroller or the other components of the board with a voltage stabilized at 5V.

Pin 3.3V, like the previous one but used in case of components that need this kind of voltage.

GND pin, corresponds to the negative pin, i.e. the mass.

Following the Arduino code, written to create a serial communication with the camera, in order to create a buffer data and process these.

```
#include <SoftwareSerial.h>  
  
SoftwareSerial mySerial(10, 11); // RX, TX  
  
void getline(char *buffer, int max_len)  
{  
    uint8_t idx = 0;  
    char c;  
    do  
    {  
        if(idx >= max_len) return;  
        while (mySerial.available() == 0) ; // wait for a char this causes the blocking  
        c = mySerial.read();  
        buffer[idx++] = c;  
    }
```



```

while (c != '\n' && c != '\r');
if(idx >= max_len) return;
buffer[idx] = 0;
}
void setup() {
Serial.begin(9600);
mySerial.begin(9600);
}
void loop(){
char buffer [63+1];
int max_len = 63;
getline(buffer, max_len);
Serial.print(buffer);
}

```

Next step will be programming also a communication between Arduino and stepper motors of the prototype, to do a double control loop and remove control desk, example Fig.53.

```

#include <Stepper.h>

const int stepsPerRevolution = 200; // change this to fit the number of steps per revolution
// for your motor

// initialize the stepper library on pins 8 through 11:
Stepper myStepper(stepsPerRevolution, 8, 9, 10, 11);

int stepCount = 0; // number of steps the motor has taken

void setup() {
  // nothing to do inside the setup
}

void loop() {
  // read the sensor value:
  int sensorReading = analogRead(A0);
  // map it to a range from 0 to 100:
  int motorSpeed = map(sensorReading, 0, 1023, 0, 100);
  // set the motor speed:
  if (motorSpeed > 0) {
    myStepper.setSpeed(motorSpeed);
    // step 1/100 of a revolution:
    myStepper.step(stepsPerRevolution / 100);
  }
}

```

Fig.53– Arduino Stepper Motor Control

Conclusion

During these months, I was commissioned to improve the design of the existing prototype at the request of the INSERM medical research team. The device must be able to perform contralateral and ipsilateral tests on more planes than the subject (sagittal plane and horizontal plane), having more control in the position of the mechanical arms. The ultimate goal is to recover the angles from these two planes, thus qualifying the proprioception of a subject.

The visual control part has been completely developed, adaptations are needed to replace ControlDesk and DSpace with Arduino. For this, I developed the serial communication program, between the camera and Arduino, and I started to develop another Arduino program, able to communicate with stepper motors and thus create a double closed loop control between camera and Arduino.

During this project I learned a lot, technical skills but also a better knowledge of project management. In fact, during real projects where you have to interact with strangers, the delays are longer, you need to anticipate certain tasks. For this reason, it was not possible to carry out many precise tests on the prototype with the new Zettlex Encoder, which arrived in the laboratory only at the end of January. In this regard I have performed geometric tests to better control the movements that can be performed with the arms.

It is necessary to work in a larger space in order to have more light or homogeneous natural light and not have difficulty in identifying the yellow colour, or to fix a small lamp on the prototype. In addition, fixing the camera on a specific support, designed and printed with 3D printing, similar to the one in Fig. 53, would make the tests faster and easier.

Once all the adjustments have been completed, to fully develop the prototype you could work on the control of trajectories not only vertical and horizontal.

This project at the Ampere Laboratory has allowed me to assimilate practical knowledge in the field of medical robotics, an area that has always fascinated me.

I am satisfied that the work done has been appreciated by my supervisor, who have followed me during the months of work, and by INSERM.

Finally, the project is being continued by another INSA's student and I am sure that the performance of the prototype will get better and better.

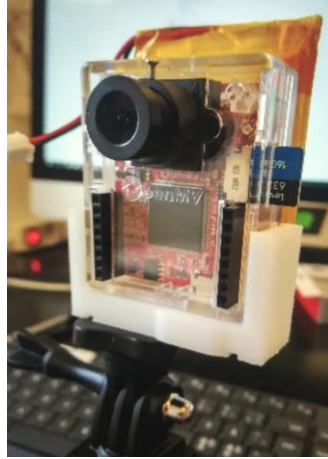


Fig.54 – Possible Camera Support

Bibliography

[1] Arnaud Ferec, Proprioception, contrôle moteur et préparation physique, Techniques de reprogrammation motrice, XavierBarbier.com, 16 Décembre 2015.

<http://www.xavierbarbier.com/proprioception-contrôle-moteur-et-preparation-physique/>

[2] Yelnik A. et al., Rééducation après accident vasculaire cérébral, EMC (Elsevier Masson SAS, Paris), Neurologie, 17-046-U-10, 2008, doi: 10.1016/S0246-0378(08)29758-7

<http://terrat.romain.free.fr/MEMOIRE/BIBLIO/ARTICLES/EMC/r%E9%99ducation%20apr%E8s%20AVC.pdf>

[3] Deriennic, F., Leclerc, A., Mairiaux, P., Meyer, J., Ozguler, A., (2000) Lombalgies en milieu professionnel : quels facteurs de risque et quelle prévention ? Paris : Institut National de la Santé et de la Recherche Médicale, [INSERM].

<http://www.ipubli.inserm.fr/bitstream/handle/10608/186/?sequence=7>

[4] Antonio Frisoli, Alberto Montagner, Luigi Borelli, Fabio Salsedo, Massimo Bergamasco, "A force-feedback exoskeleton for upper limb rehabilitation in Virtual Reality", Applied Bionics and Biomechanics", 6(2) , 2009, p. 115-126

<http://percro.sssup.it/~antony/papers/journal/AppliedBiomechanics2010.pdf>

[5] Biomécanique. R. LEPERS, A. MARTIN. éd. Ellipses. 2012

[6] The Proprioceptive Senses: Their Roles in Signaling Body Shape, Body Position and Movement, and Muscle Force, Uwe Proske, Simon C. Gandevia, Physiological Reviews Oct 2012, 92 (4) 1651-1697; DOI: 10.1152/physrev.00048.2011

[7] Jia Han, Gordon Waddington, Roger Adams, Judith Anson, Yu Liu, Assessing proprioception: A critical review of methods, Journal of Sport and Health Science, Volume 5, Issue 1, March 2016, Pages 80-90, ISSN 2095-2546, <http://dx.doi.org/10.1016/j.jshs.2014.10.004>.

[8] FISIOTEK LT-G XRI006, Catalogue de Chine Sport, Italie 2017.

<http://www.chinesport.com/catalogue/rehabilitation-equipment/continuous-passive-motion-upper-limbs/XRI006-fisiotek-lt-g/>

[9] Christina T. Fuentes, Amy J. Bastian, Where Is Your Arm? Variations in Proprioception Across Space and Tasks, *Journal of Neurophysiology* Jan 2010, 103 (1) 164-171; DOI:10.1152/jn.00494.2009

<http://jn.physiology.org/content/103/1/164>

[10] Mitsuo Kawato, ATR Human Information Processing Research Laboratories and Kawato Dynamic Brain Project, Internal models for motor control and trajectory planning, 1999.

[11] Habib, Maki K. "Handbook of Research on Advancements in Robotics and Mechatronics (2 Volumes)." IGI Global, 2015. 1-994. Web. 2 May. 2017. DOI:10.4018/978-1-4666-7387-8

[12] G. Rosati et. al., Design of a new 5 d.o.f. wire-based robot for rehabilitation, *Proceedings of the 2005 IEEE 9th International Conference on Rehabilitation Robotics*, June 28 - July 1, 2005, USA

http://smpp.northwestern.edu/ICORR2005/proceedingsCD/pdf/files/papers/ThP01_24.pdf

[13] X. Jin et. al., Upper Limb Rehabilitation Using a Planar Cable-Driven Parallel Robot with Various Rehabilitation Strategies, *Cable-Driven Parallel Robots*, Volume 32 of the series *Mechanisms and Machine Science* pp 307-321, 15 August 2014, DOI 10.1007/978-3-319-09489-2_22

https://link.springer.com/chapter/10.1007%2F978-3-319-09489-2_22

[14] BOP Charles. *Traité de robotique. Volume 3 - La partie commande*. Ellipses, 2012, 408 p. (Technosup) ISBN 2729874062

[15] P. Dario, C. Laschi, A. Menciassi, E. Guglielmelli, M. C. Carrozza, M. Zecca, L. Zollo, G. Teti, L. Beccai, F. Vecchi, S. Roccella, A Human-like Robotic Manipulation System Implementing Human Models of Sensory-Motor Coordination, CRIM (Center for

Research In Microengineering), ARTS Lab (Advanced Robotics Technology and Systems Laboratory), 2003, Pontedera (Pisa), Italy

[16] Associazione Italiana Automazione e Misura, Linee Guida per Encoder rotativi, Associazione Italiana Automazione e Misura, Novembre 2011, Italy

[17] Michael I. Voight, J. Allen Hardin, Turner A. Blackburn, Steve Tippett, Gary C. Canner, The Effects of Muscle Fatigue on and the Relationship of Arm Dominance to Shoulder Proprioception. *Journal of Orthopaedic & Sports Physical Therapy*, June 1996.

[18] Charalambos Papaxanthis, Thierry Pozzo, Marco Schieppati, Trajectories of arm pointing movements on the sagittal plane vary with both direction and speed. October 2002.

[19] Robert J. van Beers, Anne C. Sittig, Jan J. Denier van der Gon, The precision of proprioceptive position sense. *Experimental Brain Research*, March 1998, Amsterdam.

[20] Robert J. van Beers, Pierre Baraduc, Daniel M. Wolpert, Role of uncertainty in sensorimotor control, The Royal Society, Sobell Department of Motor Neuroscience and Movement Disorder, Institute of Neurology, University College London, July 2002, London UK.

[21] Zixiang Weng, Jianlei Wang, T. Senthil, Lixin Wu, Mechanical and thermal properties of ABS/montmorillonite nanocomposites for fused deposition modeling 3D printing, *Journal Elsevier*, April 2016, Fuzhou, China.

[22] D.M. Wolpert, M. Kawato, Multiple paired forward and inverse models for motor control, *Neural Network* 11 1317-1329, 1998.

[23] R.C. Miall, D. M. Wolpert, Forward Models for Physiological Motor Control, *Neural Networks* Vol.9 No. 8 pp. 1265-1279 Elsevier Science, 1996, Great Britain.

[24] Alfred C. Schouten, *Proprioceptive reflexes and neurological disorders*, 2004, The Netherlands.

[25] C. Anglin, U.P. Wyss, Review of arm motion analyses, *Proc Instn Mech Engrs* Vol 214 Part H, 1999, Switzerland.

[26] Ruth E. Mayagoitia, Anand V. Nene, Peter H. Veltink, Accelerometer and rate gyroscope measurement of kinematics: an inexpensive alternative to optical motion analysis systems, *Journal of Biomechanics* 35 (2002) 537–542, November 2001.

[27] G.A. Apker, C.P. Karimi, C.A. Buneo, Contributions of vision and proprioception to arm movement planning in the vertical plane, *Neuroscience Letters* 503 (2011) 186–190, June 2011.

[28] CIELAB Color space

https://en.wikipedia.org/wiki/CIELAB_color_space

[29] Proprioception, <https://en.wikipedia.org/wiki/Proprioception>

[30] UP Mini Plus 2, <https://www.tiertime.com/up-plus-2/>

[31] ABS (Acrylonitrile - butadiene - styrene)

<https://dielectricmfg.com/knowledge-base/abs/>

[32] Fused Deposition Modeling

https://en.wikipedia.org/w/index.php?search=Fused+filament+fabrication&title=Special%3ASearch&go=Go&wprov=acrw1_0

[33] Internal model (motor control)

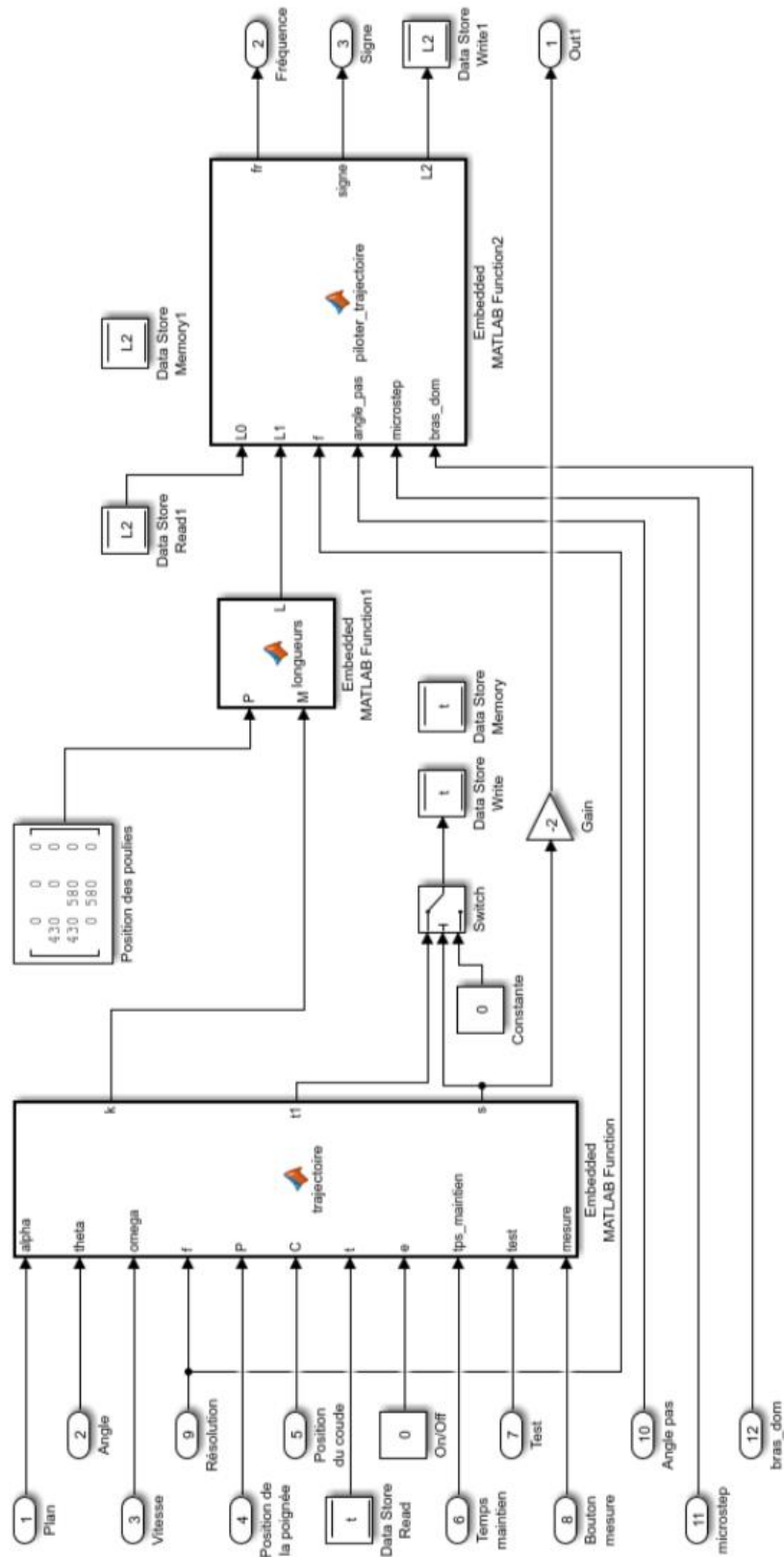
[https://en.wikipedia.org/wiki/Internal_model_\(motor_control\)](https://en.wikipedia.org/wiki/Internal_model_(motor_control))

[34] What is proprioception?, <https://sciencebeta.com/proprioception/>

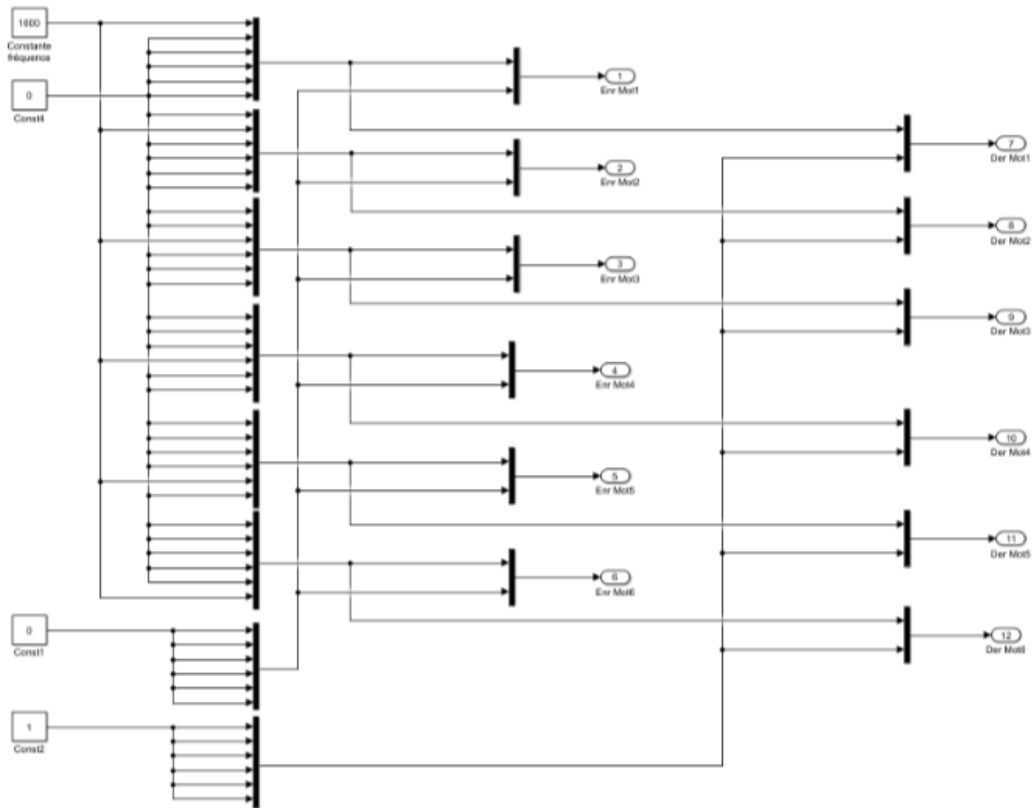
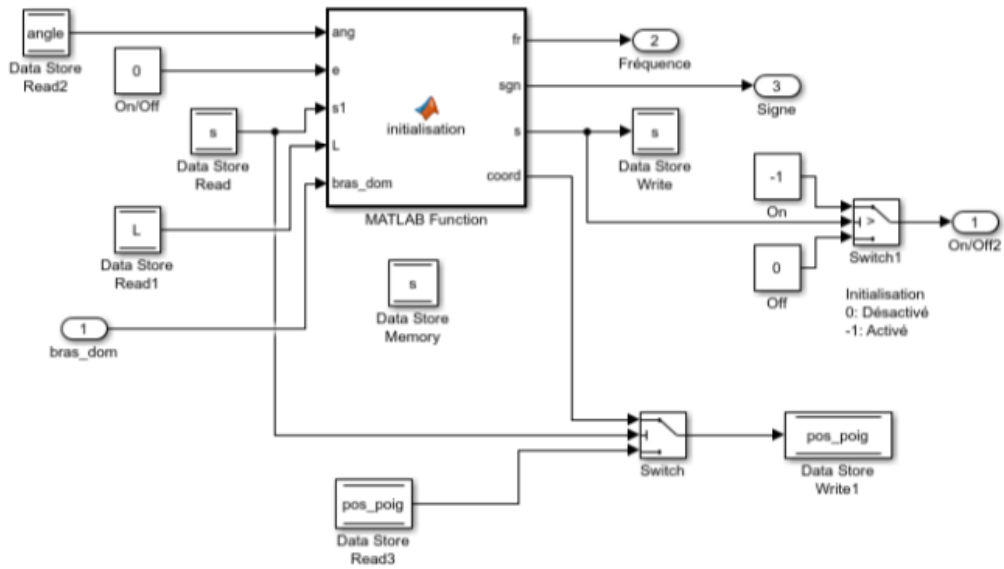
[35] OpenMV Cam M4 V1, <https://openmv.io/collections/cams/products/openmv-cam-m4-v1>

Appendix

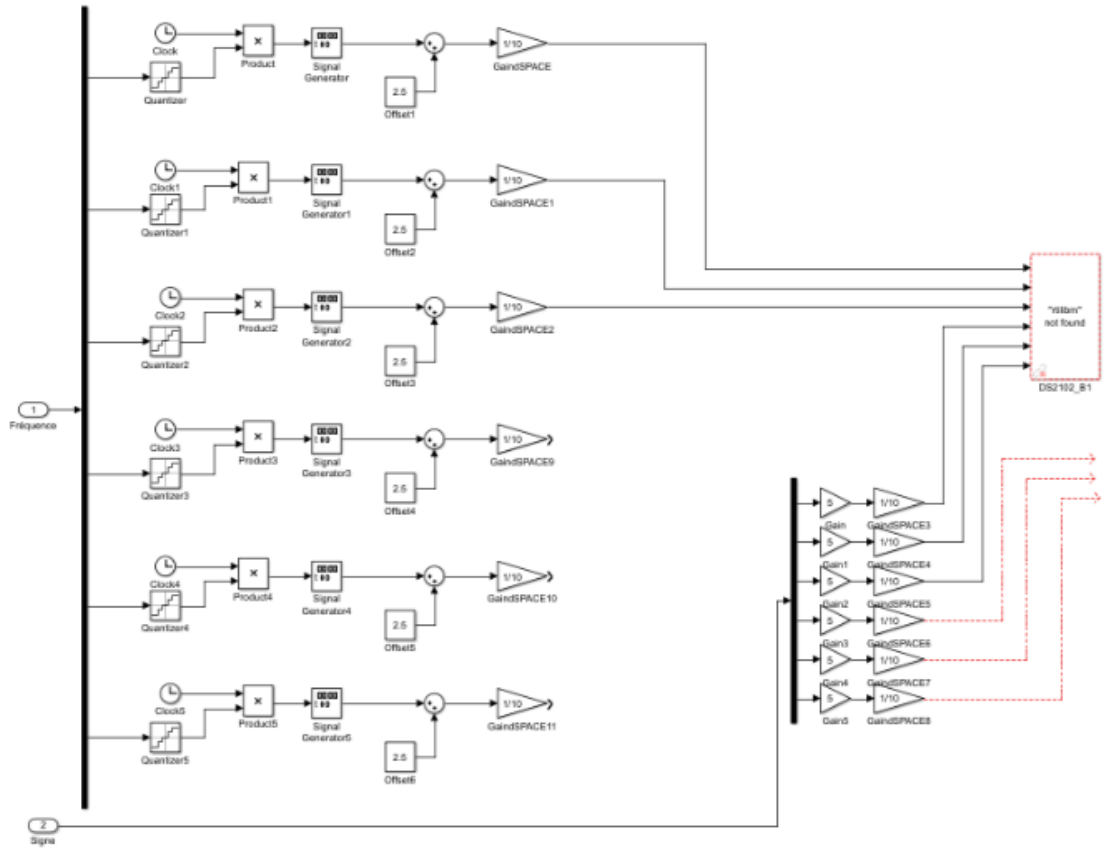
“Trajectories” subsystem



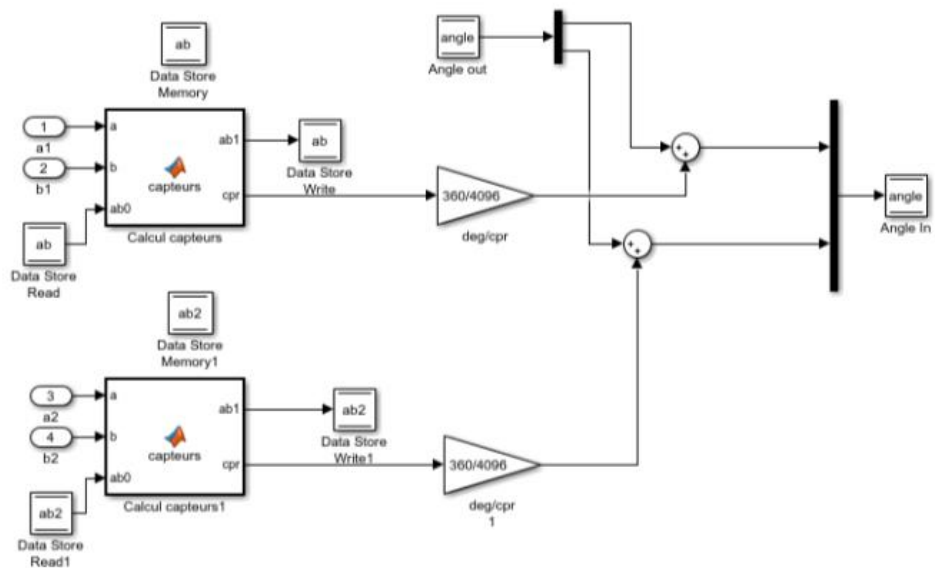
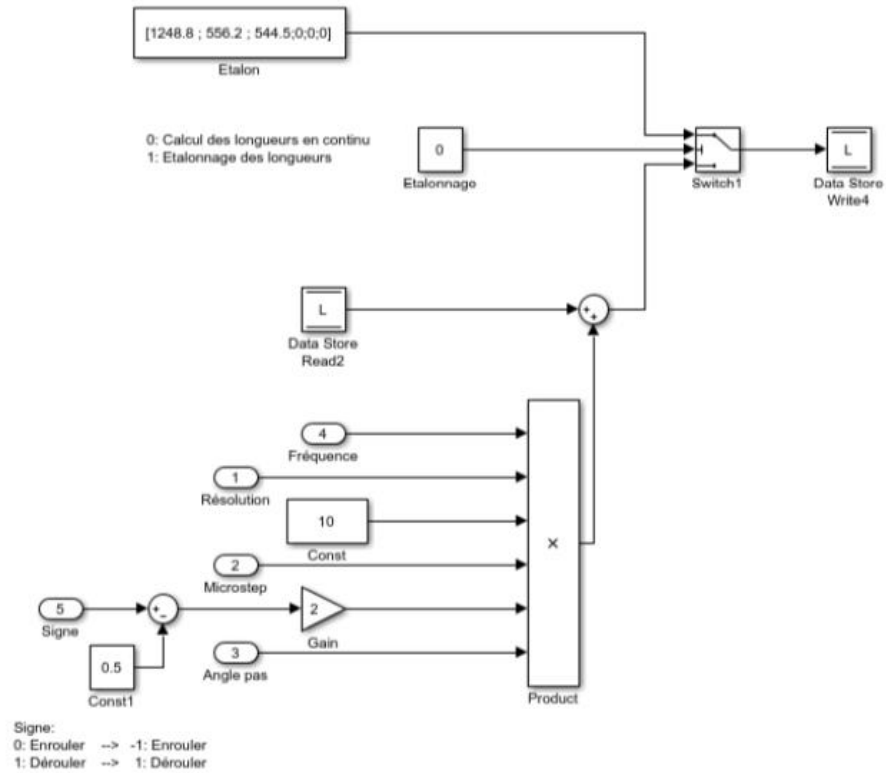
“Initialization” and “Rewind – Unwind” Subsystems



Motor Core Control Subsystem



“Lengths” and “Angles” Subsystems



Appreciation

This project would not have been possible without all the people who have been with me over the past year.

Je voudrais tout d'abord remercier le Laboratoire Ampère, mais surtout Minh Tu Pham et Richard Moreau pour m'avoir fait sentir à l'aise pendant ces mois, pour m'avoir accueillie et aidée dès le premier jour. Ils ont été deux personnes fondamentales pour mon parcours de croissance, car ils m'ont donné la possibilité de travailler et d'aborder mon étude avec un nouveau point de vue.

Je vous suis reconnaissant pour vous avoir rencontré.

È arrivato il momento di unire i puntini. Si fa così per diventare grandi. Mi guardo indietro e il disegno è un quadro astratto incomprensibile: la linea più lunga, costante e tormentata che le mie mani abbiano mai tracciato. Mi guardo indietro e la vedo quella linea, tremolante e decisa, cancellata, spezzata e ripresa. Credo sia stato l'anno più imprevedibile della mia vita e mai avrei immaginato di raggiungere questo obiettivo, dopo cinque anni intensi, in questo modo.

Quando sono partita per Lione non ero pronta a lasciare casa, i miei amici, la città in cui sono cresciuta, la città in cui studiavo, insomma tutti i posti e le persone che ti fanno sentire al sicuro. Ma alla fine sono partita, perché dentro di me sapevo che forse avevo bisogno di crescere, o forse solo non potevo mollare tutto all'ultimo così. Un misto fra malinconia e sensi di colpa.

Appena arrivata avrei solo voluto un armadio più grande, avrei voluto anche saper fare le lavatrici, capire dov'ero, chi fossi davvero e perché intorno a me sentivo solo gente che pronunciava suoni gutturali incomprensibili.

Ho iniziato a dover contare solo su me stessa. Lì ho realizzato che a casa da sempre ho accanto persone che mi vogliono bene e forse non l'ho mai detto troppo spesso.

Un grazie ai miei genitori e a mio fratello non basta. Grazie per accettare ogni giorno il mio continuo voler "scappare", per tutti gli scatoloni e i traslochi che ancora dovrò fare. Grazie per aver sempre creduto in me, per avermi incoraggiata a raggiungere i miei

obiettivi, senza dubitare un attimo che non potessi farcela. Grazie per tutti i sacrifici fatti. Grazie perché posso solo immaginare quanto sia stata dura per voi la lontananza durante la pandemia. Grazie per avermi coccolata e sostenuta nei momenti di sconforto, quando le difficoltà sembravano insormontabili, spingendomi a non mollare mai. Grazie, perché senza di voi non sarei mai diventata la persona che sono oggi.

Grazie per essere il mio faro sempre.

Grazie ai miei amici di sempre, un po' cambiati un po' gli stessi. Siete il mio punto fermo dove poter tornare, al riparo dalle tempeste.

Grazie alle mie amiche Giulietta, Agnese, Marta e Chiara. Grazie per essere sempre lì, per accogliermi con scoop e qualche bicchiere di vino. Sempre pronte ad abbracciarmi, ascoltarmi e capirmi. Grazie per essere le mie fans numero1, per sostenermi in ogni momento e in ogni scelta. Grazie per non avermi mai fatta sentire sola anche quando ero lontana.

Grazie a Edoardo, per creder in me da sempre, più di quanto non facessi io stessa. Grazie per rendere speciale tutto ciò che ti circonda. Grazie per l'amicizia eterna che ci lega. Grazie per essere stato il primo a spronarmi ad affrontare un'esperienza lontana da casa. Grazie per essere dal primo giorno il mio esempio di pura libertà.

Grazie a Lorenzo, per essermi a fianco sempre, ormai da non so più quanto tempo. Grazie per le camminate infinite quando avevamo bisogno l'una dell'altro per schiarisci le idee. Grazie per tutte le insicurezze condivise e superate insieme.

Grazie a Giorgia, per essere capace di farmi sorridere in qualunque momento con una sola parola in barese. Grazie per tutti i momenti di spensieratezza, per la focaccia bella unta e i consigli che non sono mai tardati ad arrivare. Grazie per essere diventata in poco tempo una persona su cui potrò sempre contare.

A Lione ho iniziato a vedere ciò che mi circondava con occhi diversi: consapevole e grata. Ho imparato quanto sia importante capire quando è necessario cambiare idea, perché non si smette mai di imparare per poter tirar fuori sempre il meglio di noi stessi.

All'inizio non ci pensavo, ma avevo appena incontrato le persone che sarebbero diventate presto la mia famiglia e ogni minimo barlume di privacy sarebbe presto scomparso per sempre.

Grazie Uagliuncielli per tutti gli abbracci arrivati al momento giusto, per le nottate a mangiare pancakes, per i pranzetti deliziosi del Grillon, per i caffè dopo pranzo condividendo i pochi biscotti italiani ancora rimasti, per le cene della Gvng5, per le birre annacquate, per i cicchetti, per il Raggaeton, per tutti i weekend passati nelle aule studio, per la pasta con i broccoli della domenica, per il riso salmone avocado e pomodorini, per essere piombati in camera mia a qualunque ora, in qualunque momento, senza avvisare; per tutte le cene con solo una piastra e bicchieri di plastica presi qua e là, per le "sudate" in palestra, per le cantate a squarciagola, per i computer nella doccia e per esserci ammalati tutti insieme alla scoperta degli sciroppi magici di Villeurbanne.

Non vi ringrazierò mai abbastanza per aver reso ogni momento indimenticabile.

Grazie per avermi insegnato ad essere felice senza un motivo preciso, per essere capaci di emozionarci tutti insieme per le piccole cose, per saper creare una festa in ogni momento, per ballare fino ad aver male alle gambe, per il disagio costante, per le situazioni più improbabili in cui ci siamo ritrovati. Grazie per essere tutti così diversamente instabili e così compatibili. Non mi abituerò mai all'idea di salutarvi, ma ogni volta sono sempre più consapevole della fortuna che ho avuto nell'incontrarvi.

Qualunque cosa succeda, in qualunque posto saremo, so di avervi sempre vicini per sentirci un po' fragili e sperduti come quando ci siamo incontrati per la prima volta al Parc de la Tête d'Or, pronti a ridere di ogni problema.

Vi voglio un bene indescrivibile.

Un grazie speciale a Martina, Sara e Luisa. Per gli hashtag, per la complicità e le risate continue. Grazie per essere capaci di portare il sole in ogni situazione, anche nei momenti

più grigi. Grazie per non avermi mai lasciato sola un secondo durante i mesi di quarantena. Grazie per aver condiviso ogni momento di questa esperienza unica.

Siempre están los que se van y los que se quedan, pero sabéis que lo que hemos creado es un vínculo que no conoce la distancia. Me di cuenta de que había conocido a un grupo de locos, con una vida llena de historias increíbles detrás de ellos. Con vosotros cada día fue un descubrimiento. Por tanto, quiero agradecer eternamente a mi Familia Gitana Española, por ser capaces de entendernos sin demasiados idiomas, pero tan sólo con una mirada, por protegerme y acariciarme siempre. Gracias por enseñarme el peor español posible. Gracias por ser capaz de crear una verdadera “Resistencia” en un momento complicado y absurdo como en el que nos encontramos. Gracias por superar juntos todas las dificultades y por todos los momentos felices de estos meses.

Y gracias por pronunciar mal mi nombre desde el primer día.

Os echo mucho de menos a todos.

None of this would have been the same without you.

Tutto ciò non sarebbe stato lo stesso senza di voi.